Inorganic Chemistry

Article

pubs.acs.org/IC

Reactivity of CuI and CuBr toward Dialkyl Sulfides RSR: From Discrete Molecular $Cu_4I_4S_4$ and $Cu_8I_8S_6$ Clusters to Luminescent Copper(I) Coordination Polymers

Michael Knorr,*[,†] Antoine Bonnot,[‡] Antony Lapprand,[†,‡] Abderrahim Khatyr,[†] Carsten Strohmann,[§] Marek M. Kubicki,*[,⊥] Yoann Rousselin,[⊥] and Pierre D. Harvey*[,‡]

[†]Institut UTINAM, UMR CNRS 6213, Université de Franche-Comté, 16 Route de Gray, 25030 Besançon, France

[§]Anorganische Chemie, Technische Universität Dortmund, Otto-Hahn-Strasse 6, 44227 Dortmund, Germany

[⊥]Institut de Chimie Moléculaire, UMR CNRS 6302, Université de Bourgogne, 9 Avenue A. Savary, 21087 Dijon, France

[‡]Département de Chimie, Université de Sherbrooke, 2500 Boulevard Université, Sherbrooke, Quebec J1K 2R1, Canada

Supporting Information

ABSTRACT: The 1D coordination polymer (CP) $[(Me_2S)_3\{Cu_2(\mu\text{-}I)_2\}]_n$ (**1**) is formed when CuI reacts with SMe_2 in *n*-heptane, whereas in acetonitrile (MeCN), the reaction forms exclusively the 2D CP $[(Me_2S)_3\{Cu_4(\mu\text{-}I)_4\}]_n$ (**2**) containing "flower-basket" Cu_4I_4 units. The reaction product of CuI with MeSEt is also solvent-dependent, where the 1D polymer $[(MeSEt)_2\{Cu_4(\mu_3\text{-}I)_2(\mu_2\text{-}I)_2\}(MeCN)_2]_n$ (**3**) containing "stepped-cubane" Cu_4I_4 units is isolated in MeCN. In contrast, the reaction in *n*-heptane affords the 1D CP $[(MeSEt)_3\{Cu_4(\mu_3\text{-}I)_4\}]_n$ (**4**) containing "closed-cubane" Cu_4I_4 clusters. The reaction of MeSPr with CuI provides the structurally related 1D CP $[(MeSPr)_3\{Cu_4(\mu_3\text{-}I)_4\}]_n$ (**5**), for which the X-ray structure has been determined at 115, 155, 195, 235, and 275 K, addressing the evolution of the metric parameters. Similarly to **4** and the previously reported CP $[(Et_2S)_3\{Cu_4(\mu_3\text{-}I)_4\}]_n$ (*Inorg. Chem.* **2010**, *49*, 5834), the 1D chain is built upon closed cubanes $Cu_4(\mu_3\text{-}I)_4$ as secondary building units (SBUs) interconnected via μ-MeSPr ligands. The 0D tetranuclear clusters $[(L)_4\{Cu_4(\mu_3\text{-}I)_4\}]$ [L = EtSPr (**6**), Pr_2S (**7**)] respectively result from the reaction of CuI with EtSPr and *n*-Pr_2S. With *i*-Pr_2S, the octanuclear cluster $[(i\text{-}Pr_2S)_6\{Cu_8(\mu_3\text{-}I)_3\}(\mu_4\text{-}I)_2\}]$ (**8**) is formed. An X-ray study has also been performed at five different temperatures for the 2D polymer $[(Cu_3Br_3)(MeSEt)_3]_n$ (**9**) formed from the reaction between CuBr and MeSEt in heptane. The unprecedented framework of **9** consists of layers with alternating $Cu(\mu_2\text{-}Br)_2Cu$ rhomboids, which are connected through two μ-MeSEt ligands to tetranuclear open-cubane Cu_4Br_4 SBUs. MeSPr forms with CuBr in heptane the 1D CP $[(Cu_3Br_3)(MeSPr)_3]_n$ (**10**), which is converted to a 2D metal−organic framework $[(Cu_5Br_5)(\mu_2\text{-}MeSPr)_3]_n$ (**11**) incorporating pentanuclear $[(Cu_5(\mu_4\text{-}Br)(\mu_2\text{-}Br)]$ SBUs when recrystallized in MeCN. The thermal stability and photophysical properties of these materials are also reported.

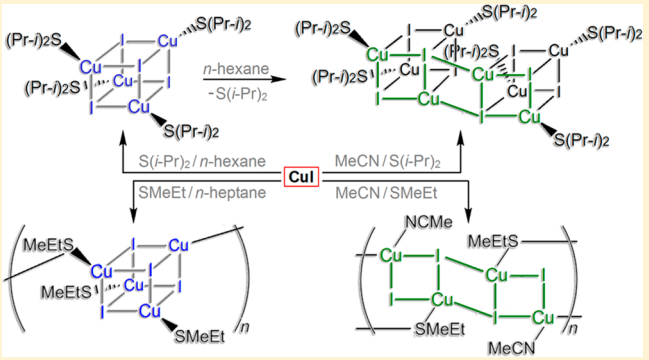

INTRODUCTION

Copper halides are known to easily form adducts with a wide range of neutral group V donor ligands such as aliphatic amines, aromatic N-containing heterocycles, organic nitriles, PR_3, AsR_3, and SbR_3.[1−6] Even organometallic species are readily formed by complexation of alkenes, alkynes, N-heterocyclic carbenes, CO, and isonitriles.[7−10] The interest in the study of CuX and CuX_2 thioether complexes started in the 1970s and was motivated, in part, by the fact that Cu−thioether and Cu−disulfide interactions occur naturally in several biological systems.[10−13] For example, (+)-biotin and the methionine residue of proteins and enzymes incorporate thioether groups, which are potential metal-bonding sites. In the blue copper redox proteins, some of the Cu atoms, either singly (type I) or in pairs (type II), apparently coordinate to one or more sulfur ligands.[14−17]

Therefore, several groups investigated in detail the coordination chemistry of CuX and CuX_2 thioether adducts as simple model compounds to provide a better understanding on the copper−sulfur interaction in biological systems.[18−21] CuCl and $CuCl_2$ complexes with Me_2S have been reported to catalyze the isomerization of dichlorobutenes.[22] The CuBr·Me_2S adduct exhibits also some applications as a reagent in organic chemistry and is commercially available as a precursor for organic transformations.[23] Recently, CuI films were used for sensing volatiles such as Me_2S, Et_2S, and tetrahydrothiophene (THT).[24] Unsurprisingly, the coordination chemistry of copper halide−thioether adducts is dominated by CuX·RSR com-

Received: February 10, 2015
Published: April 6, 2015

DOI: 10.1021/acs.inorgchem.5b00327
Inorg. Chem. 2015, 54, 4076−4093

Chart 1. Representation of Some Common CuX·L Motifs[a]

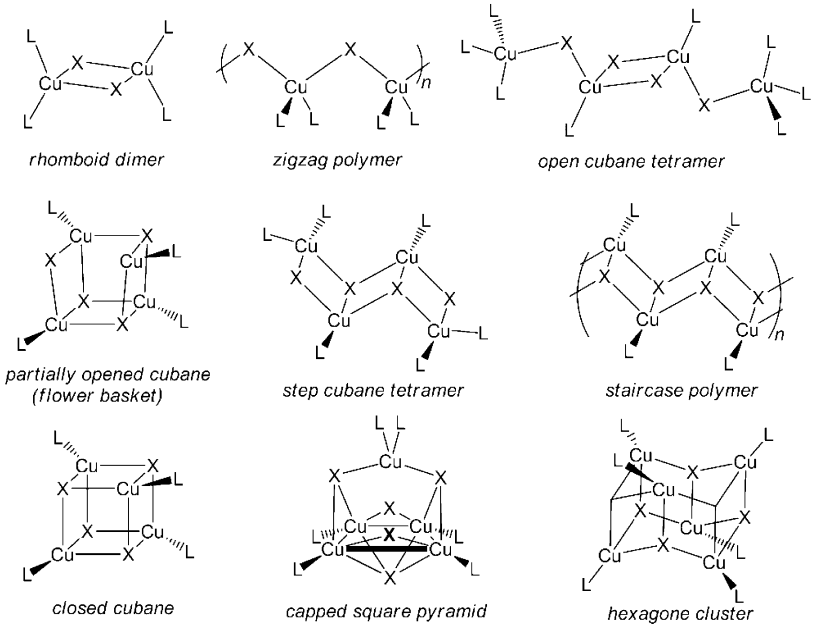

[a]The di- and polynuclear cluster units may be assembled by additional bonding Cu···Cu interactions, if d(Cu···Cu) is close to or below the sum of the van der Waals radii (2.8 Å) of two Cu atoms.

pounds. In accordance with the hard and soft acids and bases principle,[25] soft thioether donors have a higher affinity for CuX salts, which are softer Lewis acids than the CuX_2 salts. Nevertheless, a few paramagnetic $CuCl_2$·RSR adducts and mixed-valence systems have been reported.[26−29] Although some rare examples of distinct (0D) mononuclear or dinuclear species such as $[CuCl(Me_2S)_3]$ and $[Cu_2I_2(THT)_4]$ are known,[30] single-crystal X-ray crystallography revealed that in the majority of cases polymeric networks are formed.[31] This tendency of thioethers to form coordination polymers (CPs) upon treatment with copper halides relies on two facts. First, copper halides tend to form readily di- or polynuclear clusters upon coordination of neutral donor ligands via the formation of μ_2- or μ_3-halide bridges. For the CuX adducts case with the general formula $Cu_nX_nL_m$, a fascinating diversity of stoichiometries and geometries has been structurally evidenced, as exemplified in Chart 1.[32,33] When the ligand and metal are reacted in a 1:1 molar ratio, the most common encountered motif consists of the tetranuclear cubane-like Cu_4X_4 cluster (mostly for X = I), in which the halide centers act as triply bridging ligands. The cubane motif may also be disrupted for the benefit of a "stepped-cubane" tetramer or an open-cubane structure when bulky ligands are used. The very rare open-cubane tetramer is derived from the "stepped-cubane" motif by breaking one of the two Cu−X bonds associated with each of the terminal Cu centers and completing the tetrahedral coordination sphere of the terminal Cu centers by ligation of another donor. Another very scarce motif is the hexagonal prism $Cu_6(\mu_3\text{-}X)_6$ cluster, which has been encountered in 2D and 3D networks as secondary building units (SBUs).[34,35] The use of a ligand in excess favors generally the formation of μ_2-bridged rhomboid dimers or the ring-opened geometry of the latter, named the "zigzag polymer". The formation of di- and polynuclear cluster cores, exhibiting in some cases Cu···Cu distances significantly less than twice the van der Waals radii of two Cu atoms (2.8 Å), may be facilitated by the so-called "cuprophilic" interactions.[36−40] Second, in contrast with PR_3, AsR_3, pyridines, and NR_3 donor ligands, simple sulfides R−S−R (also called dialkyl sulfanes) dispose on two nonbonding lone pairs on the S atom, allowing a bridging μ_2-bonding mode; in other words, the thioether S atom can also act as a four-electron donor in the solid state.

The first report on the rational preparation of copper(I) coordination polymers (CPs) of this type stems from Potenza et al., who reacted CuX salts with Et_2S and discovered that the reaction with CuI produces a complex with a ligand-to-copper ratio of 3:4.[3] This unusual stoichiometry of the Et_2S adduct was revealed by X-ray diffraction, which evidenced the formation of the 1D CP $[(Et_2S)_3\{Cu_4(\mu_3\text{-}I)_4\}]_n$. Its structure consists of infinite chains of sulfide-bridged Cu_4I_4 cubane-like cores built from the interpenetration of two Cu_4 and I_4 tetrahedra. Because $Cu_4I_4L_4$ clusters often exhibit an intense emission,[4] we recently reexamined the structural features and photophysical properties of this compound and indeed noticed the presence of an intense luminescence. We also evidenced that the nature of the halide may also have a crucial influence on the framework structure because the self-assembly reaction of SEt_2 with CuBr results in a 1D polymer of composition $[(Cu_3Br_3)(SEt_2)_3]_n$.[43a] The framework of the latter polymer is quite different from that of the CuI·Et_2S adduct and consists of a corrugated array with alternating $Cu(\mu_2\text{-}Br)_2Cu$ rhomboids. These latter units are connected through two bridging SEt_2 ligands to a tetranuclear open-cubane Cu_4Br_4 SBU, ligated on two external Cu atoms with one terminal SEt_2. Intrigued by the structural richness and interesting photophysical properties of these apparently simple CuX·RSR adducts, we extended our investigation on the complexation of other symmetric and dissymmetric aliphatic monothioethers such as SMe_2, SPr_2, $S(i\text{-}Pr)_2$, MeSEt, MeSPr, and EtSPr. We now report on the impact of the alkyl substituent, the nature of the halide and solvent on the architecture, and the photophysical properties of the new compounds. In some cases, unprecedented structural motifs

DOI: 10.1021/acs.inorgchem.5b00327
Inorg. Chem. 2015, 54, 4076−4093

Chart 2. Drawing of the Structures of the Various Polymers Formed between CuX and SMe_2

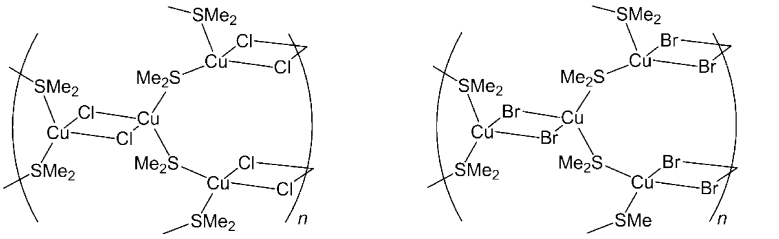

2D $[(Me_2S)_2\{Cu_2(\mu_2\text{-}Cl)_2\}]_n$ (d Cu···Cu 2.983(1) Å) 2D $[(Me_2S)_2\{Cu_2(\mu_2\text{-}Br)_2\}]_n$ (d Cu···Cu 2.951(4) Å)

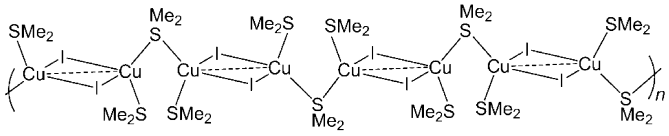

1D $[(Me_2S)_3\{Cu_2(\mu_2\text{-}I)_2\}]_n$ (d Cu···Cu 2.684(1) Å) (**1**)

have been evidenced. Furthermore, this in-depth study is accompanied by several X-ray structure determinations at variable temperatures. These analyses have been carried out with the aim of obtaining a deeper insight into the temperature-dependent evolution of the metric parameters such as the Cu···Cu distances and the volumes of Cu_4 and I_4 tetrahedra. A small part of this work was recently communicated.[43b]

RESULTS AND DISCUSSION

1. Coordination of SMe_2 on CuI. Several groups have previously investigated the complexation of dimethyl sulfide on CuX salts. If CuCl is dissolved in neat SMe_2, the mononuclear adduct $[CuCl(SMe_2)_3]$ can be isolated after crystallization at low temperature.[30a] As stated, in 1975 Potenza et al. investigated the complexation of CuI and CuBr in neat SMe_2 and isolated 1:1 complexes according to elemental analyses.[41] In the early 1990s, both groups of van Koten and Mälger reported a similar series of reactions with SMe_2 and were able to determine their structures by X-ray diffraction studies of the $CuCl{\cdot}Me_2S$, $CuBr{\cdot}Me_2S$, and $CuI{\cdot}Me_2S$ adducts.[44,45] The data revealed the formation of CPs consisting of layered 2D networks for both $[(\mu\text{-}Me_2S)_2\{Cu_2(\mu_2\text{-}Cl)_2\}]_n$ and $[(\mu\text{-}Me_2S)_2\{Cu_2(\mu_2\text{-}Br)_2\}]_n$. The 1D chain $[(Me_2S)_3\{Cu_2(\mu\text{-}I)_2\}]_n$ (**1**) with a 2:3 CuI-to-Me_2S ratio was obtained by the direct treatment of CuI in neat dimethyl sulfide and the subsequent crystallization induced by the addition of *n*-hexane. For the latter, the cubane cluster encountered in $[(Et_2S)_3\{Cu_4(\mu_3\text{-}I)_4\}]_n$ was replaced by the rhombic Cu_2I_2 unit, which exhibits a rather short Cu···Cu distance of 2.684(1) Å (Chart 2 and Scheme 1, reaction a).

Scheme 1. Preparation of Polymers 1 and 2

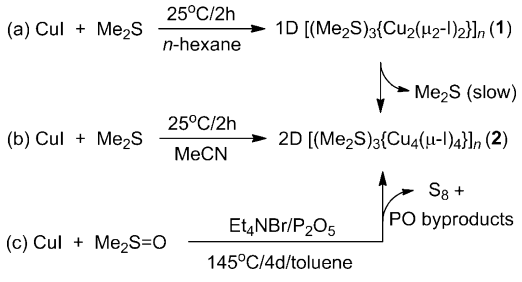

More recently, Dai et al. demonstrated that a unique 2D double-layered CP with composition $[(Me_2S)_3\{Cu_4(\mu\text{-}I)_4\}]_n$ (**2**) containing helical chains can be constructed under solvothermal conditions in the presence of dimethyl sulfoxide (Scheme 1, reaction c).[46]

The production of SMe_2 is explained by the deoxygenation of Me_2SO by P_2S_5. According to Dai et al., the same reaction with CuBr or CuCl under identical conditions led to the formation of 2D polymers $[(\mu\text{-}Me_2S)_2\{Cu_2(\mu_2\text{-}X)_2\}]_n$ incorporating rhomboid $Cu(\mu\text{-}X)_2Cu$ (X = Br, Cl) units (Chart 2).[46a] A single-crystal X-ray analysis of the polymer $[(Me_2S)_3\{Cu_4(\mu\text{-}I)_4\}]_n$ (**2**) revealed that it has a 2D structure, in which two μ-Me_2S ligands assemble distinct Cu_4I_4 clusters (Scheme S1 in the Supporting Information, SI). In contrast with the "closed" cubane-like $Cu_4(\mu_3\text{-}I)_4$ core encountered for 1D $[(Et_2S)_3\{Cu_4(\mu_3\text{-}I)_4\}]_n$, the Cu_4I_4 unit in the 2D CP **2** is named by the authors as "flower-basket-shaped" because it can be described as a partially opened structural variation of the widespread closed bis-tetrahedral Cu_4I_4 motif.[46] Figure 2 (bottom, left) shows that within the core motif of **2** three Cu atoms are placed in an isosceles trigonal arrangement, which is located in the waist position of the flower basket. The fourth Cu atom (up) lies at the handle position of the flower basket bridging two I atoms.

In order to study the luminescence properties of the CP **1**, we prepared this compound according to the protocol of Mälger et al.[45] No luminescence was noticed upon examination of a freshly prepared crystalline sample under a UV black light lamp at 366 nm. However, we noticed rapidly the occurrence of luminescent spots after exposure to air. Despite the use of dry crystalline samples, the characteristic repugnant smell of volatile dimethyl sulfide was noticed, indicating a transformation. When revisiting a sample kept in a closed vial 4 weeks later, we noticed a profound modification of the emission feature of the colorless solid, which was now strongly emissive under UV light (Figure S1 in the SI). A comparison of the emission spectra with those reported for **2** revealed that in the solid-state slow evaporation of Me_2S had quantitatively transformed non-emissive polymer **1** into emissive polymer **2**. Similar facile phase transformations were recently reported for CuI complexes ligated by the volatile THT ligand.[24b]

In order to evaluate the solvent effect on the material composition, a saturated solution of CuI in acetonitrile

DOI: 10.1021/acs.inorgchem.5b00327
Inorg. Chem. 2015, 54, 4076−4093

(MeCN) at ambient temperature was reacted with a 5-fold excess of SMe_2 according to Scheme 2. After the reaction

Scheme 2. Reaction of CuI and MeSEt in MeCN and *n*-Heptane, Respectively Forming 3 and 4

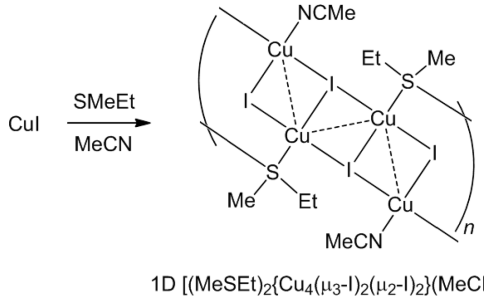

1D $[(MeSEt)_2\{Cu_4(\mu_3\text{-}I)_2(\mu_2\text{-}I)_2\}(MeCN)_2]_n$ **3**

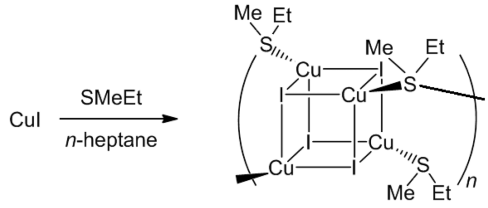

1D $[(MeSEt)_3\{Cu_4(\mu_3\text{-}I)_4\}]_n$ **4**

mixture was cooled, the formation of colorless crystals was observed. Surprisingly, the single-crystal X-ray analysis performed at 115 K revealed that, instead of the expected 1D CP **1** being observed, the 2D polymer **2** was formed as the sole species. Selected crystal data of **2** recorded at 115 K are given in ref 46b. The Cu···Cu distances vary from 2.665(3) to 2.715(3) Å with a mean value of 2.688 Å. This last value is essentially the same as that observed in the 173 K structure (2.690 Å) reported by Dai et al.[46a]

2. Coordination of MeSEt with CuI. In order to evaluate the impact of the steric parameters and the nature of the solvent on the topology of the frameworks of the polymers, CuI was reacted in both a MeCN solution and *n*-heptane with MeSEt. Mixing a saturated solution of CuI in MeCN with a 3-fold excess induced after several hours the formation of large colorless needle-shaped crystals, which were isolated in 68% yield (Scheme 2). The attenuated total reflectance infrared spectrum of this solid exhibits two adsorption bands at 2998 and 2268 cm^{-1}, indicating the presence of Cu-bound MeCN ligands.

Indeed, an X-ray diffraction study of **3** confirmed the coordination of two MeCN molecules per SBU. The polymeric compound $[(MeSEt)_2\{Cu_4(\mu_3\text{-}I)_2(\mu_2\text{-}I)_2\}(MeCN)_2]_n$ (**3**) forms an infinite 1D ribbon running along the *a* axis in the $P2_1/c$ space group and does not consequently bring any particular symmetry. The ribbons consist of Cu_4I_4 SBUs of the "stepped-cubane" type, which are interconnected through two bridging MeSEt ligands (Figure 1). Although the "stepped-cubane" Cu_4I_4 core has been encountered as a motif in $[Cu_4(\mu_3\text{-}I)_2(\mu_2\text{-}I)_2\}(2\text{-}Mepy)_6]$ and a $Cu_4I_4(L_n)_2$ cluster supported by the chelating 4,4′-(1,2-phenylene)bis(1-benzyl-1*H*-1,2,3-triazole) ligand,[47,48] compound **3** constitutes the first example of a CuX● monothioether-linked CP incorporating the "stepped-cubane"-type cluster as a SBU. There are two types of Cu^I centers, which are connected through a loose Cu1···Cu1 contact of 2.8719(6) Å and two shorter Cu1···Cu2 interactions

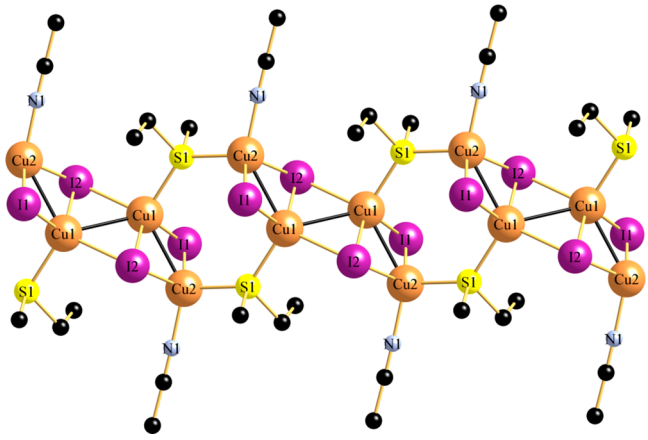

Figure 1. View of a segment of the MeSEt-bridged 1D ribbon of **3** along the *a* axis. The H atoms are omitted for clarity. Selected bond lengths (Å) and angles (deg): Cu1−Cu1#1 1 2.8719(6), Cu1−Cu2 2.7042(4), Cu1−S1 2.3337(6), Cu2−S1#2 2.3317(6), Cu1−I1 2.6505(3), Cu1−I2 2.6289(4), Cu1#1−I2 2.6744(4), Cu2−I1 2.5967(4), Cu2−I2 2.6691(3), Cu2−N1 1.999(2), C1−N1 1.139(3). Symmetry transformations used to generate equivalent atoms: #1, 1 − *x*, 1 − *y*, 1 − *z*; #2, −*x*, 1 − *y*, 1 − *z*.

of 2.7042(4) Å. This indicates that, in fact, there are two Cu_2I_2 rhomboids bridged through two μ_3-I2 atoms with the formation of a new central rhomboid. The dihedral angle of the Cu2−Cu1−Cu1−Cu2 array amounts to 180°. The μ_2-bridging I1 atom spans the Cu1 and Cu2 ions with a slight asymmetry of 0.05 Å (Figure 1), whereas the I2 atom bridges Cu2, Cu1, and Cu1#1 in a μ_3-bonding mode with Cu−I bond lengths of 2.6691(3), 2.6289(4), and 2.6744(4) Å, respectively. Each Cu2 ion bears an extra MeCN ligand. The interconnection between the Cu_4I_4 SBUs is secured by a μ_2-bound MeSEt ligand bridging the Cu1 and Cu2 ions of two adjacent SBUs, thus forming six-membered cycles comprising the S1−Cu1−Cu2−S1−Cu1−Cu2 atoms. Both the Cu_4I_4 SBUs and the six-membered rings lie over the symmetry centers.

A different type of CP was obtained when using the noncoordinating solvent *n*-heptane. CuI was first solubilized in neat MeSEt. At the end of the exothermic reaction, the clear solution was layered with *n*-heptane. Slow diffusion occurring over several days allowed the growth of colorless block-shaped crystals in 66% yield. Diffraction data recorded on the strongly luminescent material were of poor quality (final *R* factor = 0.0991). Consequently, another crystallization has been attempted, but once more the crystals were of similarly low quality (R = 0.1012). The *Pbca* space group was found for both crystals with essentially the same low precision on bond distances [estimated standard deviation (esd) of 0.004 Å for Cu···Cu and of 0.04 Å for C−C]. However, the formation of a 1D polymer, $[(MeSEt)_3\{Cu_4(\mu_3\text{-}I)_4\}]_n$ (**4**), is unambiguously confirmed. Its structure is reminiscent of that of the previously studied $[(Et_2S)_3\{Cu_4(\mu_3\text{-}I)_4\}]_n$ consisting of a 1D array of tetranuclear Cu_4I_4 clusters, which are aligned by two bridging μ_2-MeSEt ligands (Figure 2, top). The chains run over *b* glide planes of the *Pbca* orthorhombic space group (Figure S2 in the SI). The coordination around each Cu_4I_4 SBU is completed by two terminal MeSEt ligands. Within the cluster core (Figure 2, bottom, right), the Cu···Cu separations range from 2.701(4) to 2.737(4) Å, averaging 2.722(6) Å at 115 K. Despite the rather low quality of the X-ray data of **4** (Table S4 in the SI), the Cu_4 tetrahedra therein are seemingly among the most regular ones

DOI: 10.1021/acs.inorgchem.5b00327
Inorg. Chem. 2015, 54, 4076−4093

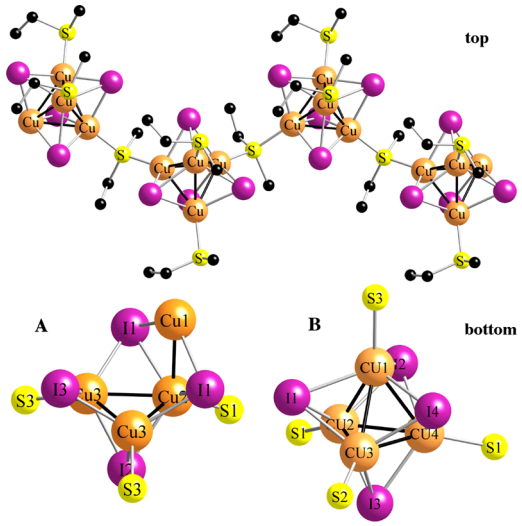

Figure 2. (top) View of a segment of the MeSEt-bridged 1D ribbon of **4** along the *b* axis. The H atoms are omitted for clarity. (bottom) Comparison between the flower-basket Cu_4I_4 core of **2** (A) and the closed-cubane Cu_4I_4 core of **4** (B).

in this work, with shortest and longest Cu···Cu distances differing only by 0.036 Å.

Like $[(Et_2S)_3\{Cu_4(\mu_3\text{-}I)_4\}]_n$ and $[(MeSPr)_3\{Cu_4(\mu_3\text{-}I)_4\}]_n$ (**5**) (see below), polymer **4** is strongly luminescent when exposed to a laboratory UV lamp at 354 nm. No aging was noticed after 2 weeks of contact with air in an open vial. In contrast, freshly prepared crystals of **3** are not emissive under 354 nm UV light. However, these crystals became rapidly opaque after exposure to air and finally crumbled during drying. Interestingly, the emission spectrum of a dried powder sample is identical with that of **4**, so that again a solid-state transformation due to evaporation of coordinated MeCN may explain this observation.[48−54]

3. Coordination of MeSPr with CuI. In order to study the impact of the alkyl chain lengths of the RSR′ ligand on the framework, CuI was also first dissolved in neat methyl propyl sulfide, and then the homogeneous mixture was layered with *n*-heptane. Suitable crystals for X-ray analysis of the luminescent 1D polymer **5** were obtained in 71% yield and subjected to a diffraction study at five different temperatures (Tables S1 and S5 in the SI). The X-ray structure of **5** at 115 K was recently communicated.[43b] The 1D ribbons run along the *b* direction in the $P2_1/c$ monoclinic space group (Figure 3) zigzagging over the 2-fold 2_1 screw axis (Figure S3 in the SI).

A graphical evolution of Cu···Cu distances at different temperatures is presented in Figure 4, while variations of the Cu_4 tetrahedron volumes will be presented in Figure 7 together with those for the structure of **7**. The mean value of Cu···Cu distances in **5** increases by 1.67% in the 160 K range (Table S1 in the SI) and corresponds to the values found for other variable-temperature studies on cubane-like Cu_4I_4 structures.[43,44,53,64b] The volume of a Cu_4 tetrahedron in **5** increases by 4.09% and that of I_4 decreases by −0.59%, in agreement with other studies.

To check whether the composition of the material is solvent-dependent, as noticed in the cases of polymers **3** and **4**, CuI was also treated with an excess of MeSPr in MeCN as the reaction medium. Homogeneous crystals were obtained in 68% yield, and their emission spectrum was identical with that of the *n*-heptane product **5**. Furthermore, the X-ray structure of the

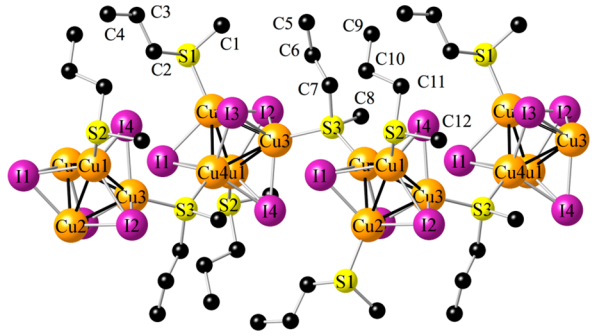

Figure 3. View of a segment of the MeSPr-bridged 1D ribbon of **5** along the *b* axis. The H atoms are omitted for clarity. Selected bond lengths (Å) and angles (deg) at 115 K: Cu1−Cu3 2.6707(6), Cu1−Cu4 2.6757(6), Cu1−Cu2 2.6954(5), Cu2−Cu4 2.7122(6), Cu2−Cu3 2.7943(6), Cu3−Cu4 2.6714(6), Cu1−S3 2.3066(8), Cu1−I3 2.6332(4), Cu1−I1 2.6381(5), Cu1−I4 2.7004(5), Cu2−S3#1 2.3197(8), S3−Cu2#2 2.3197(8), Cu3−S2 2.3059(9), Cu4−S1 2.2990(9), Cu2−I4 2.6494(4), Cu2−I2 2.6664(4), Cu2−I3 2.6703(4), Cu3−I2 2.6823(5), Cu3−I1 2.7020(5), Cu3−I4 2.7271(5), Cu4−I1 2.6572(5), Cu4−I2 2.6962(5), Cu4−I3 2.7259(5); Cu4−Cu1−Cu2 60.658(15), Cu1−Cu2−Cu3 58.188(14), Cu1−Cu3−Cu4 60.114(16), Cu3−Cu4−Cu2 62.531(15), S3−Cu1−I1 103.37(2), S3#1−Cu2−I4 107.09(2), S2−Cu3−I2 107.80(3), S1−Cu4−I1 110.72(3), Cu1−I1−Cu4 60.700(13), Cu2−I2−Cu3 62.990(13), Cu1−I3−Cu2 61.088(13), Cu2−I4−Cu1 60.499(12). Symmetry transformations used to generate equivalent atoms: #1, $-x-1, y-{}^1/_2, -z-{}^3/_2$; #2, $-x-1, y+{}^1/_2, -z-{}^3/_2$.

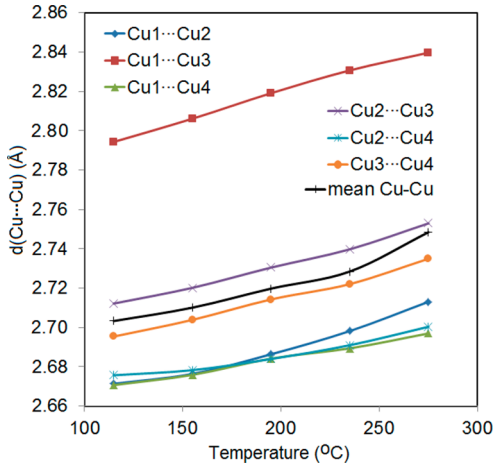

Figure 4. Temperature dependence of the Cu···Cu distances (Å) for **5**.

product, which crystallized from MeCN was determined at 173 K and was found to be that of **5**.

4. Coordination of EtSPr on CuI. A surprising structural change occurred when the chain lengths of the Et−S−R ligand was extended to *n*-propyl. After dissolution of CuI in neat ethyl propyl sulfide and layering of the homogeneous mixture with *n*-heptane, colorless crystals were isolated in 73% yield. Surprisingly, elemental analysis indicated a 1:1 metal-to-ligand ratio. Indeed, X-ray diffraction analysis performed at 115 K (Table S4 in the SI) revealed that, instead of the anticipated tetranuclear cluster-containing polymer, the discrete 0D cluster $[(EtSPr)_4\{Cu_4(\mu_3\text{-}I)_4\}]$ (**6**) formed. The cluster has a crystallographic 2-fold symmetry over the axis at 0, *y*, $^1/_4$. The cluster core is constructed of four Cu centers, which are connected through Cu···Cu distances ranging from 2.6821(16) to

DOI: 10.1021/acs.inorgchem.5b00327
Inorg. Chem. 2015, 54, 4076−4093

2.829(2) Å (Figure 5). The mean Cu···Cu contact of 2.728 Å compares well with those of other tetranuclear closed-cubane

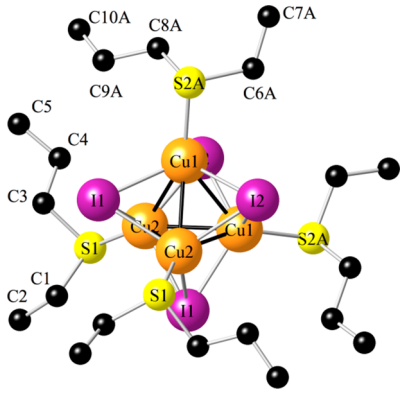

Figure 5. Molecular structure of the cluster **6**. Only the major ligand A is shown. The H atoms are omitted for clarity. Selected bond lengths (Å): Cu1−Cu1#1 2.726(2), Cu1−Cu2 2.7246(17), Cu1−Cu2#1 2.6821(16), Cu2−Cu2#1 2.829(2), Cu1−S2A 2.310(4), Cu1−S2B 2.364(9) (not shown), Cu2−S1 2.308(3), Cu1−I1 2.6835(13), Cu1−I3 2.6826(15), Cu1−I3#4 2.7004(13), Cu2−I1 2.6740(13), Cu2−I1#4 2.6875(14), Cu2−I2#1 2.6570(13). Symmetry transformations used to generate equivalent atoms: #1, $-x, y, -z + {}^{1}/_{2}$.

cores incorporated as assembling nodes in polymeric networks assembled by dithioether or macrocyclic thiacrown ethers.[33] Like in polymers **4** and **5**, each Cu_3 face is capped by a μ_3-iodo ligand, with a Cu−I distance varying from 2.6570(13) to 2.7004(13) Å. Each Cu atom is ligated by a terminal thioether ligand. The volume of a Cu_4 tetrahedron in **6** (2.386 $Å^3$) is greater than that in **5** (2.324 $Å^3$), whereas that of a I_4 tetrahedron (**6**: 10.367 $Å^3$) is smaller (**5**: 10.394 $Å^3$). Such an inversed correlation of tetrahedral volumes Cu_4 versus I_4 constitutes a general trend within the family of closed-cubane-like Cu_4I_4 structures.[43a,64b] Performing the synthesis in MeCN had, in this case, no impact on the molecular structure. A comparison of the cell parameters of crystals grown from MeCN revealed again the *Pbcn* orthorhombic space group.

Although the discrete $[L_4\{Cu_4(\mu_3\text{-}I)_4\}]$ motif is quite common for L = PR_3, AsR_3, Py, and NR_3, we are aware of only two other examples of molecular $[(R_2S)_4\{Cu_4(\mu_3\text{-}I)_4\}]$ clusters. The first, with composition $[(DodSMe)_4\{Cu_4(\mu_3\text{-}I)_4\}]$ (Dod = $C_{12}H_{25}$), has been obtained, together with the iodocuprate salt $[DodMe_2S][(DodSMe)_3(Cu_3I_4)]$, by the treatment of CuI with the salt dodecyldimethylsulfonium iodide ($[DodMe_2S]I$).[54] Within the unit cell of this $Cu_4I_4S_4$ cluster [mean Cu···Cu contact of 2.741(1) Å at 299 K], the intermolecular interactions between the long $C_{12}H_{25}$ substituents give rise to a laminar organization of interpenetrating dodecyl chains. During the preparation of this manuscript, Pike et al. reported the structures of two polymorphs of $[(THT)_4\{Cu_4(\mu_3\text{-}I)_4\}]$, whose Cu···Cu distances lie in the ranges 2.673(2)−2.761(2) and 2.639(3)−2.768(3) Å, repectively.[24b]

The strongly luminescent crystalline product **6** is air-stable but starts to soften above 298 K and melted during hot summer days to give a yellowish liquid. In the liquid state, the luminescence almost vanished under UV light at 366 nm but reappeared when a sample solidified upon recooling. This reversibility of the luminescence indicates that the cluster does not disintegrate, at least entirely, after fusion and recooling. No cycling was performed to see whether this stability was sustained.

5. Coordination of SPr_2 with CuI. In their seminal paper, San Fillippo et al. also briefly described in their experimental section a large-scale reaction involving 0.23 mol of CuI in 0.46 mol of neat SPr_2.[41] They isolated a yellow-orange liquid, whose elemental analysis indicated a 1:2 copper-to-ligand ratio, suggesting the composition $[(Pr_2S)_2(CuI)]$. Because of this intriguing result, this reaction was revisited using a somewhat modified experimental procedure. First, CuI was dissolved in an excess of SPr_2, and then this clear solution was layered with *n*-hexane. After storage at 5 °C, large amounts of colorless crystals formed on the wall of the *n*-hexane phase after 1 day. However, isolation of the pure material was hampered at temperatures above 20 °C during removal of the solvent. Indeed, the crystals melted slowly, forming a viscous liquid. As observed for cluster **6**, luminescent compound $[(Pr_2S\text{-}n)_4\{Cu_4(\mu_3\text{-}I)_4\}]$ (**7**) is not emissive as a liquid but becomes again strongly luminescent after solidification upon placement of a sample in a freezer. A comparison of the powder X-ray diffraction patterns of a sample before melting with a hair dryer and a solidified sample confirms that the Cu_4I_4 cluster of **7** (see below) has been restored. After several attempts, single crystals of sufficient quality for X-ray analysis were extracted from a cooled sample and subjected to X-ray diffraction study at 115, 155, 195, and 235 K (Tables S2 and S6 in the SI). Structure elucidation at 115 K (Figure 6) revealed the discrete molecular cluster **7**, for which the overall structure is quite similar to that of **6**.

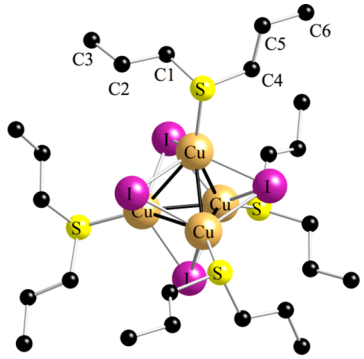

Figure 6. Molecular structure of cluster **7** at 115 K. H atoms are omitted for clarity. Selected bond lengths (Å): Cu1···Cu1#1 2.6299(15), Cu1···Cu1#2 2.9043(16), Cu1···Cu1#3 2.9503(16), Cu1−S1 2.3151(18), Cu1−I1 2.6695(9), Cu1−I1#1 2.6767(9), Cu1−I1#2 2.6932(9). Symmetry transformations used to generate equivalent atoms: #1, $-x, y, -z + {}^{1}/_{2}$; #2 $-x, -y + {}^{1}/_{2}, z$; #3 $x, -y + {}^{1}/_{2}, -z + {}^{1}/_{2}$.

The molecule lies on the intersection of three 2-fold axes in the *Ccca* orthorhombic space group and has the crystallographic local symmetry D_2-222. Consequently, there are one Cu, one I, and one S atoms in the asymmetric unit. Within the dissymmetric tetranuclear cluster core, the Cu···Cu distances range from 2.6299(15) to 2.9503(16) Å, with an average Cu···Cu contact of 2.828 Å. There is an unexpected and curious variation of the Cu···Cu distances and volumes within the Cu_4 and I_4 tetrahedra as a function of the temperature depicted in Figure 7 for the volumes of Cu_4. For compound **5**, a roughly monotonic increase of the Cu_4 volumes is observed (see also Figure 4), but the situation dramatically changes for **7**, for

DOI: 10.1021/acs.inorgchem.5b00327
Inorg. Chem. 2015, 54, 4076−4093

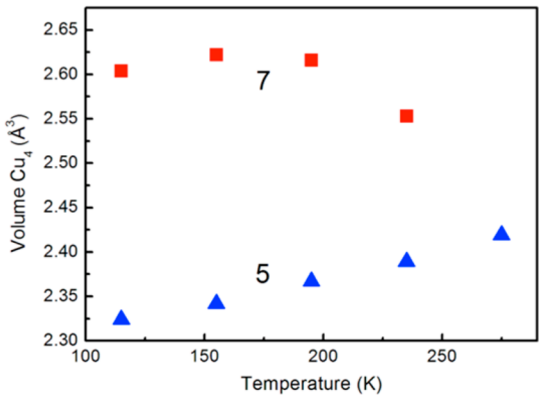

Figure 7. Temperature dependence of $V(Cu_4)$ for **5** and **7**.

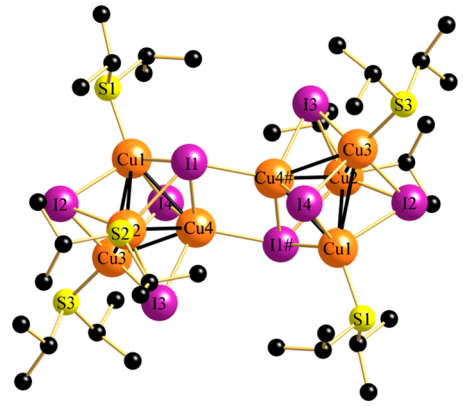

Figure 8. Molecular structure of cluster **8a** at 173 K. H atoms are omitted for clarity. Selected bond lengths (Å): Cu1···Cu2 3.0757(9), Cu1···Cu3 3.1578(9), Cu1···Cu4 2.8952(9), Cu2···Cu3 3.0483(7), Cu2···Cu4 2.7875(9), Cu3···Cu4 2.9114(8) Cu4···Cu4#1 3.0730(6), Cu1−S1 2.2945(10), Cu2−S2 2.2987(9), Cu3−S3 2.3055(9), Cu1−I1 2.7138(6), Cu1−I2 2.6798(9), Cu1−I4 2.6161(6), Cu2−I1 2.8138(9), Cu2−I2 2.6096(7), Cu2−I3 2.6736(7), Cu3−I2 2.6908(7), Cu3−I3 2.6965(7), Cu3−I4 2.6918(9), Cu4−I1 2.6402(6), Cu4−I3 2.6454(9), Cu4−I4 2.6402(6), I1−Cu4#1 2.6862(8). Symmetry transformations used to generate equivalent atoms: #1, $-x + 1$, $-y + 2$, $-z + 1$.

which the evolution of the metric parameters does not follow the usual monotonic variations neither for the Cu···Cu distances (overall decrease by 1.1%) nor for the $V(Cu_4)$ volumes (Table S4 in the SI). The trends in the evolution of the volumes are also inversed, where an overall decrease of $V(Cu_4)$ (−2.0%) and an increase of $V(I_4)$ (+3.5%) upon warming are noted. This phenomenon is not due to a phase transition because the space group and the sets of equivalent positions remain the same. This observation may be rather related to a low melting point of **7**, a factor already mentioned above.

6. Coordination of S(*i*-Pr)$_2$ with CuI. To address the impact of steric crowding of the sulfide ligand (*n*-Pr vs *i*-Pr) on the cluster nuclearity, CuI was also dissolved in an excess of S-*i*-Pr_2 and then layered with *n*-hexane. In the early stage of the crystallization process, the formation needle-shaped colorless crystals was noticed on the wall of the *n*-hexane phase. Unfortunately, the crystal became rapidly opaque after drying, so no crystal of suitable quality could be obtained. On the basis of the similarity of the emission spectrum with those of **6** and **7**, the formation of a tetranuclear cluster, $[(i\text{-}Pr_2S)_4\{Cu_4(\mu_3\text{-}I)_4\}]$, is suggested. When the sample was placed inside a Schlenk tube, the onset of a slow growth of large block-shaped transparent crystals commenced, the quantity of which increased over several days. These types of block-shaped crystals were the dominant species when a higher CuI-to-ligand ratio was used. X-ray diffraction revealed that, instead of isolation of a second polymorphic tetranuclear compound (as reported for $[(THT)_4\{Cu_4(\mu_3\text{-}I)_4\}]$),[24b] the cluster $[(i\text{-}Pr_2S)_6\{Cu_8(\mu_3\text{-}I)_3\}(\mu_4\text{-}I)_2\}]$ (**8a**) was formed. Figure 8 shows that this rare motif can be considered as an octanuclear cluster consisting of two fused centrosymmetric Cu_4I_4 cores, which are linked through two μ_4-iodo ligands. The Cu_4 tetrahedron is quite irregular because the Cu···Cu distances range in a large interval between 2.7875(9) and 3.1578(9) Å. The average Cu···Cu contact of 2.9794 Å is far above the sum of the van der Waals radii of two Cu atoms and markedly superior to those of **4**−**7**. This mean value exceeds even that for the 2D polymer $[Cu_4I_4\{\mu\text{-}t\text{-}BuS(CH_2)_4S\text{-}t\text{-}Bu\}_2]_n$ in which the cubanes are linked by the bulky t-BuS$(CH_2)_4$S-*t*-Bu ligand [Cu···Cu 2.911(2) Å].[55] The connectivity to the second Cu_4 cluster is performed by two μ_4-bridging I1 ligands, with a loose Cu···Cu contact of 3.0730(6) Å (Figure 8). Compound **8a** represents the first example of a molecular sulfur-ligated CuI cluster with this structural octanuclear motif. We are aware of only one example of a somewhat related 3D metal−organic framework (MOF), $[(Cu_4I_4)_2\{\mu\text{-}BzS(CH_2)_4SBz\}_3]_n$ [*d*(Cu···Cu) 2.81 Å at 293 K], in which two Cu_4I_4 clusters share a single common μ_4-iodo ligand.[56] Moreover, there is also an example of a 3D 2-fold-interpenetrated MOF assembled by nitrogen-containing ligands and incorporating Cu_8I_8 clusters, namely, $[Cu_{14}I_{14}(dabco)_5(py)]_n$ (dabco = 1,4-diazabicyclo[2.2.2]-octane; py = pyridine).[57,58] This luminescent material contains both $Cu_6I_6N_6$ clusters of the hexagon prism type and $Cu_8I_6N_6$ clusters as SBUs.[57a] The latter can be regarded as similar to **8a** in which double-cubane Cu_4I_4 clusters are linked together by two Cu−I bonds. However, the Cu···Cu distances, ranging from 2.6484(15) to 2.831(2) Å, are significantly shorter than that found in **8a**.

In order to verify whether there is a solvent influence on the structural motif, as encountered for the CPs **1**/**2** and **3**/**4**, we also reacted CuI with an excess of S(*i*-Pr)$_2$ in MeCN as the solvent. Colorless large crystals of this highly soluble compound were obtained from a concentrated solution and analyzed by X-ray diffraction analysis. The crystallographic data from the crystals grown in MeCN were identical with those obtained from *n*-hexane (triclinic space group $P\bar{1}$; Table S4 in the SI). This result rules out a solvent effect directing formation of the octanuclear structure of cluster **8a**.

One obvious question then arises: why does the reaction of CuI with S(*n*-Pr)$_2$ lead to a $Cu_4I_4S_4$ cluster, whereas with S(*i*-Pr)$_2$, a $Cu_8I_8S_6$ cluster is formed? Because the electron-donating properties of *n*-Pr and *i*-Pr can be considered as quasi-identical, the different outcomes must most likely be due to the enhanced steric crowding exerted by the *i*-Pr substituents compared to the linear *n*-Pr groups. This steric argumentation may be comparable to the well-established cone-angle concept developed by Tolman for PR_3 ligands (taking into account the presence of a lone pair on the S atom as the third substituent).[59] The unexpected formation of **8a** may be rationalized by an initial formation of a cubane-type cluster, $[(i\text{-}Pr_2S)_4\{Cu_4(\mu_3\text{-}I)_4\}]$ (**8b**), which by the dissociation of one S(*i*-Pr)$_2$ ligand minimizes steric crowding (Scheme 3).

DOI: 10.1021/acs.inorgchem.5b00327
Inorg. Chem. 2015, 54, 4076−4093

Scheme 3. Formation of Tetranuclear (8b) and Octanuclear (8a) Clusters

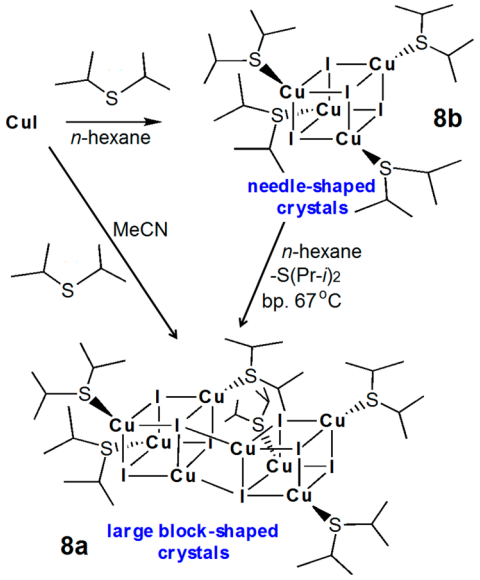

7. Coordination of MeSEt with CuBr. We recently demonstrated that the structure of the 1D CP $[(Cu_3Br_3)(SEt_2)_3]_n$ formed upon complexation of SEt_2 with CuBr is quite different from its CuI counterpart.[43a] The architecture of the former polymer consists of centrosymmetric rhomboid $Cu_2(\mu\text{-}Br)_2$ dimers with a Cu3···Cu3 distance of 3.0454(7) Å, which are linked to a distorted open-"stepped-cubane" Cu_4Br_4 motif by two μ-SEt_2 ligands in an alternating manner [the Cu2···Cu1 and Cu2···Cu2 distances respectively average 2.7311(5) and 3.0125(8) Å], thus giving rise to an infinite 1D chain (Figure 9A).

Because copper-containing CPs incorporating two different inorganic core motifs are very rare, we were intrigued whether upon using MeSEt as the ligand a material with a "conventional" framework like that in the 2D $[\{Cu_2(\mu_2\text{-}Br)_2(\mu\text{-}Me_2S)_2\}]_n$ polymer would be formed (above) or whether a MOF incorporating a more "exotic" inorganic SBU core would be isolated. Indeed, single crystals were obtained by layering a solution of CuBr in neat MeSEt with *n*-heptane, and crystallographic characterization of a colorless crystal of composition $[(Cu_3Br_3)(MeSEt)_3]_n$ (**9**) was made. The X-ray data revealed some structural similarities for the SBUs with those of $[(Cu_3Br_3)(SEt)_3]_n$, but a change in the dimensionality upon going from 1D to 2D was noted. Each **9** layer is constructed from alternating rhomboid Cu_2Br_2 dimers (Cu1··· Cu4 3.074 Å) and open-"stepped-cubane" Cu_4Br_4 units, which are linked through two μ_2-MeSEt ligands, thus forming a distorted six-membered cycle (Figure 9B and Tables S3 and S7 in the SI). The coordination sphere around Cu1 is completed by a terminal MeSEt thioether. The 2D connectivity within the layer is achieved by a third μ_2-MeSEt ligand linking Cu1 and Cu2 of the neighbored Cu_4Br_4 units (Figure S4 in the SI). The "stepped-cubane" fragment lies over the symmetry center ($^1/_2$, 0, 1) of the $P2_1/c$ space group.

Each Cu_4Br_4 unit consists of two rhomboid $[Cu(\mu_2\text{-}Br)(\mu_3\text{-}Br)Cu]$ dimers with a Cu2−Cu3 distance of 2.7831(13) Å at 115 K. The two rhomboids are loosely interconnected through two μ_3-bromide ligands [Cu3−Br4 2.5026(12) Å]. The separation between neighboring Cu3 centers of this tetranuclear core amounts to 3.274 Å. A crystallographic study at five different temperatures has also been performed, and the variations of the Cu···Cu distances with the temperature are given in Table S3 in the SI and Figure 10. The shortest distance between two neighboring Cu2 and Cu3 atoms from the "stepped-cubane" tetrameric unit, which is close to the sum of the van der Waals radii, increases, as expected, as the

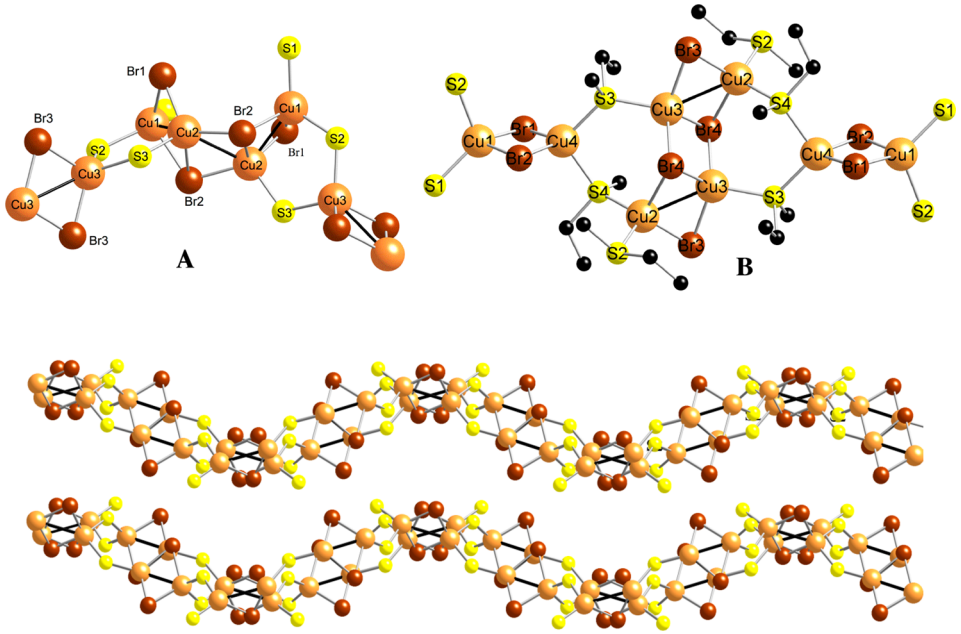

Figure 9. (top) Comparison between the SEt_2-bridged motif of $[(Cu_3Br_3)(SEt_2)_3]_n$ (A)[43a] and the MeSEt-bridged motif of **9** incorporating alternating dinuclear $Cu_2(\mu\text{-}Br)_2$ and tetranuclear $Cu_4(\mu\text{-}Br)_4$ units along the *b* axis (B). (bottom) View down the *c* axis on the *ab* plane of a segment of **9** showing the undulating arrangement of the layers. The alkyl groups are omitted for clarity. A view down the *a* axis on the *bc* plane of this 2D polymer is presented in Figure S4 in the SI.

DOI: 10.1021/acs.inorgchem.5b00327
Inorg. Chem. 2015, 54, 4076−4093

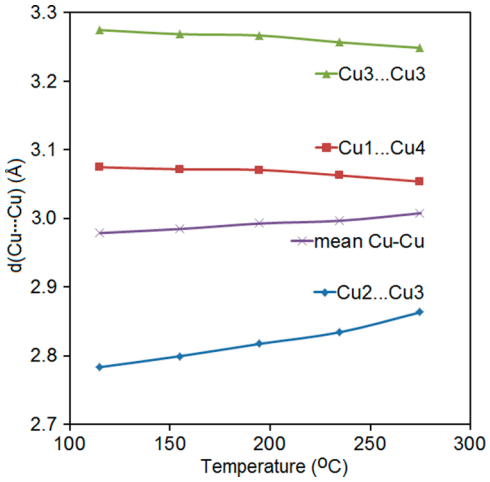

Figure 10. Temperature dependence of the Cu···Cu distances in **9**.

temperature rises. This is also consistent with what is generally observed for the iodo derivatives (except for **7**, as discussed above). Conversely, both long Cu···Cu distances slightly shorten when the temperature is increased. The overall average Cu···Cu distance increases by 1% due to a rather strong increase of the short Cu2···Cu3 distances (+2.9%) and a smooth decrease of the long Cu1···Cu4 (−0.7%) and Cu3···Cu3#1 (−0.8%) distances.

8. Coordination of MeSPr with CuBr. A framework of composition $[(Cu_3Br_3)(MeSPr)_3]_n$ (**10**) containing alternating dinuclear Cu_2Br_2 rhomboids and Cu_4Br_4 SBUs of the open-"stepped-cubane" type was generated when a solution of CuBr was layered in neat MeSPr with *n*-heptane. Crystallographic characterization of the large colorless crystals isolated after slow diffusion revealed that, despite the similar overall composition, there are some striking structural differences between **9** and **10**. In contrast to the 2D MOF **9**, the CP **10** is organized in 1D ribbons (Figure 11 and Table S4 in the SI). These are constructed by centrosymmetric rhomboid $Cu_2(\mu\text{-Br})_2$ dimers with a Cu1···Cu1#1 distance of 2.8995(5) Å, which are linked through four μ_2-MeSPr ligands to two neighboring open-"stepped-cubane" Cu_4Br_4 units. Thus, the connectivity between the two SBUs differs from that of the CP **9**. Each Cu_4Br_4 SBU consists of two rhomboid $[Cu(\mu_2\text{-Br})(\mu_3\text{-Br})Cu]$ dimers with a Cu2−Cu3 distance of 2.7854(4) Å. The two rhomboids are loosely interconnected through two μ_3-bromide ligands. Together with a very loose contact of 3.233 Å between two opposite Cu3 centers, this connectivity gives rise to a centrosymmetric open-"stepped-cubane" Cu_4Br_4 core. The coordination sphere around Cu2 is completed by a terminal MeSPr thioether. Despite the different dimensionalities of the CPs **9** and **10**, the Cu···Cu distances are similar in the tetrameric SBUs of both compounds: Cu2···Cu3, 2.7831(13) versus 2.7854(4) Å, and Cu3···Cu3′, 3.274 versus 3.233 Å, respectively, at 115 K. Figure S5 in the SI shows that the 1D chains run in directions parallel to the lattice [−1 1 0] ones and diagonal between the *a* and *b* vectors. We are not aware of this kind of alternating linkage between a dinuclear species and a tetranuclear species in other CuBr-containing CPs.

A remarkable framework transformation occurs when **10** is recrystallized from a MeCN solution. A 2D MOF with a hitherto unprecedented $[(Cu_5Br_5)(\mu_2\text{-MeSPr})_3]_n$ (**11**) framework incorporating pentanuclear $[(Cu_5(\mu_4\text{-Br})(\mu_3\text{-Br})_2(\mu_2\text{-Br})_2]$ SBUs is obtained (Figure 12). Structural features and

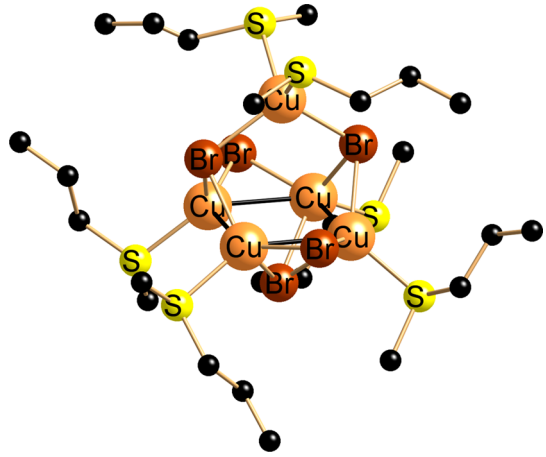

Figure 12. View of the pentanuclear cluster core of **11**.[43b]

photophysical data of this material have been recently reported by us;[43b] therefore, these data are not presented again herein. This finding demonstrates again that the choice of the solvent may be of crucial importance during the crystallization process. The fact that MeCN molecules are found within the channels

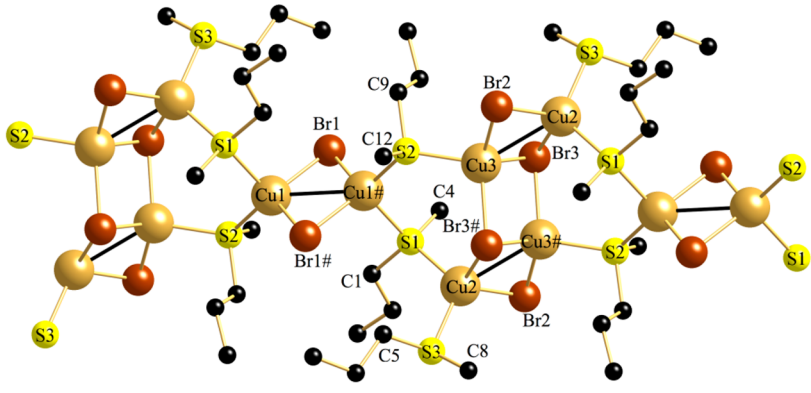

Figure 11. View of a segment of the ribbon of the 1D polymer **10** at 115 K. H atoms are omitted for clarity. Selected bond lengths (Å): Cu1−Cu1#1 2.8995(5), Cu2−Cu3 2.7854(4), Cu3−Cu3#2 3.233, Cu1−Br1 2.4508(4), Cu1−Br1#1 2.4729(4), Cu2−Br2 2.4420(4), Cu2−Br3 2.6150(4), Cu3−Br2 2.4705(3), Cu3−Br3 2.4963(3), Cu3−Br3#2 2.5180(4), Cu1−S1 2.3219(5), Cu1−S2 2.2604(4), Cu2−S1 2.2802(5), Cu2−S3 2.2634(6), Cu3−S2 2.3103(5). Symmetry transformations used to generate equivalent atoms: #1, −*x*, −*y* + 3, −*z*; #2, −*x* + 1, −*y* + 2, −*z*.

DOI: 10.1021/acs.inorgchem.5b00327
Inorg. Chem. 2015, 54, 4076−4093

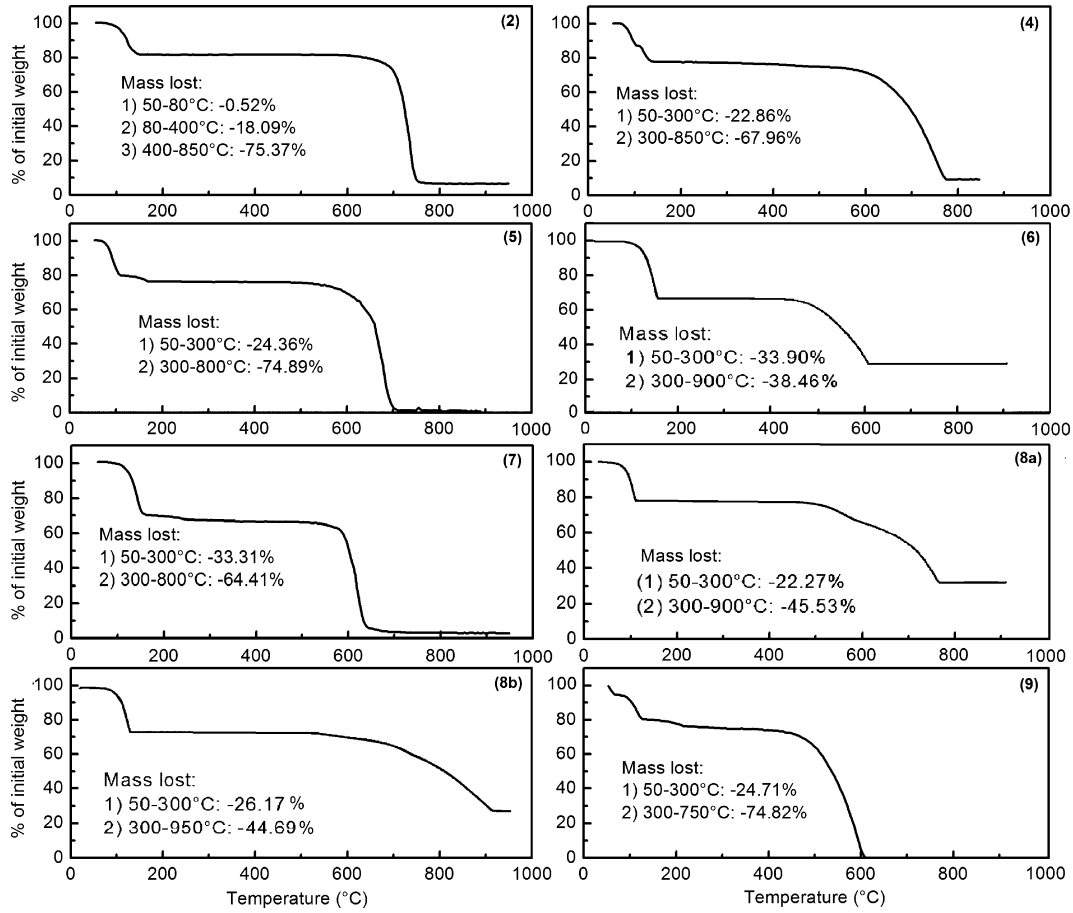

Figure 13. TGA traces of **2**, **4**, **5**, **6**, **7**, **8a**, **8b**, and **9** (10 °C/min; N_2, 50 mL/min).

of this zeolite-like framework may very likely account for the solvent dependence of the outcome.

9. Thermal Stability. The thermal behavior for the CPs **2**, **4**, **5**, **6**, **7**, **8a**, **8b**, and **9** was addressed by thermogravimetric analysis (TGA). The first derivative plots of the TGA traces are given in Figure S6 in the SI. Generally, all of the TGA traces exhibit similar thermal behavior and present three distinct plateaus (Figure 13 and Table S8 in the SI). The first plateau ranges from 25 and ∼100 (±40) °C. The temperatures of decomposition, characterized by a loss of 5% of the total mass, are given in Table S8 in the SI. These data indicate that these CPs are relatively fragile upon increasing the temperature. At higher temperatures, a large mass loss is observed, presumably caused by the decomposition of the ligand. At temperatures in the vicinity of ∼150 to ∼500−600 °C, a second plateau is observed, but the range depends upon the sample. Finally, upon further heating, another weight loss occurs and leads to a final plateau. This last plateau can be attributed to a metal-containing residual or a complete evaporation of all of the volatile products when the final mass approaches 0%. Specific details are provided below.

The first weight loss occurring between ∼60 and 160 °C corresponds to decreases of 18.5, 22.5, 22.4, 33.9, 33.3, 22.3, 26.2, and 24.7% for **2**, **4**, **5**, **6**, **7**, **8a**, **8b**, and **9**, respectively. The theoretical values accounting for the mass loss of the first ligand over the total mass of **2**, **4**, **5**, **6**, **7**, **8a**, **8b**, and **9** are respectively 19.7, 22.3, 26.2, 35.4, 38.3, 31.8, 38.3, and 34.7%, which relatively match for **2** and **4**−**6**. In these cases, it is reasonable to assign this first thermal event to a ligand loss of the CP. For **7**, **8a**, **8b**, and **9**, the recorded mass loss is larger than what theory predicts for the loss of one ligand and one can assume that this thermal process is associated with a ligand decomposition/reaction. It is worth noting that these CPs exhibit relatively low thermal stability (Table S8 in the SI) and may be linked to the fact that these ligands have rather low boiling points. These ligand boiling points are ∼38, ∼66, ∼91, ∼117, ∼142, ∼120, and ∼96 °C for Me_2S (**2**), MeSEt (**4** and **9**), Et_2S (**5**), EtSPr (**6**), Pr_2S (**7**), *i*-Pr_2S (**8a** and **8b**), and MeSPr (**10**), respectively.

The second weight losses present a different feature depending on the compounds. The mass losses in the ranges ∼600 to ∼750 (**2**), ∼550 to ∼780 (**4**), ∼520 to ∼750 (**5**), ∼450 to ∼600 (**6**), ∼520 to ∼650 (**7**), ∼500 to ∼760 (**8a**), ∼520 to ∼700 (**8b**), and ∼450 to ∼600 °C (**9**) total 75.4, 68.0, 74.9, 38.5, 64.9, 45.5, 44.7, and 74.8%, respectively. For **5**, **7**, and **9**, the weight loss is total, meaning that the final decomposition organometallic products are volatile at these temperatures. For the other CPs, two trends are noted. For **2** and **4**, an almost total vaporization is observed, but residuals of respectively 6.0 and 9.2% are depicted in the TGA traces, which most probably result from copper metal. Finally, the last decomposition processes occurring for **6**, **8a**, and **8b** match perfectly with the theory, i.e., the loss of total weight of the halide atoms: 38.5 (42.9), 45.5 (45.3), and 44.7 (41.0% in theory), respectively. Their residual masses correspond to Cu atoms because the observed masses [27.6 (21.6), 32.2 (22.9), and 29.1 (20.6% in theory)] match relatively well with the expected theoretical values.

DOI: 10.1021/acs.inorgchem.5b00327
Inorg. Chem. 2015, 54, 4076−4093

10. Photophysical Studies. The CP **2** contains a "flower-basket" SBU, and a strong emission appears at ∼549 nm (Figure 14, left). The position and the emission lifetime, τ_e

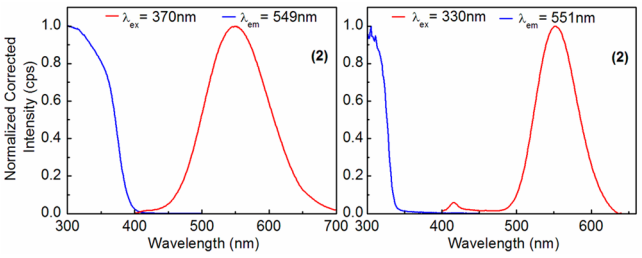

Figure 14. Emission (red) and excitation (blue) spectra of the CP **2** at 298 (left) and at 77 K (right).

Table 1. Emission Maxima (λ_{max}, nm) and Corresponding Lifetime Values (τ_e, μs)[a]

	298 K		77 K	
compd	λ_{max}, nm	τ_e, μs (λ_{em}, nm)	λ_{max}, nm	τ_e, μs (λ_{em}, nm)
2	549	5.04 ± 0.04 (570)	551	15.71 ± 0.23 (570)
4	550	4.66 ± 0.04 (560)	540	11.55 ± 0.25 (560)
5	544	6.74 ± 0.25 (560)	535	8.49 ± 0.09 (540)
6	623	2.57 ± 0.01 (43%)	667	1.93 ± 0.01 (16%)
		5.17 ± 0.01 (27%) (590)		2.08 ± 0.01 (84%) (590)
7	618	3.57 ± 0.01 (85%)	601	1.02 ± 0.01 (95%)
		12.75 ± 0.01 (15%) (600)		3.51 ± 0.01 (5%) (600)
8a	573	0.20 ± 0.01 (580)	542	0.26 ± 0.01 (49%) (580)
				2.69 ± 0.01 (51%)
8b	526	0.45 ± 0.01 (540)	503	2.12 ± 0.01 (47%) (530)
				3.34 ± 0.01 (46%)
9	442	<0.1 (380)	440	4.98 ± 0.07 (370)
				8.29 ± 0.20 (510)

[a] λ_{em}: wavelength used for the τ_e measurements.

(5.04 ± 0.04 μs; Table 1), are consistent with a cubane-like species.[35,43] Upon cooling, the emission band shifts slightly to ∼551 nm (Figure 14, right), and τ_e increases to 15.71 ± 0.23 μs. Other examples of strongly emissive closed cubanes are provided for the CPs **4** and **5** and clusters **6** and **7**. The resemblance of the photophysical properties between **2** and **4** indicates that the closed-cubane and flower-basket structures exhibit similar behavior.

The longer lifetime is consistent with an increase in the medium rigidity, and the red shift upon going from 549 to 551 nm between 298 and 77 K may very likely witness a decrease in the Cu···Cu distances, as occasionally illustrated above for other species upon cooling.

The CPs **4** and **5** exhibit similar optical features where two emission bands can be depicted at low temperature (Figure 15). Indeed, both CPs exhibit broad, intense, and red-shifted emissions in the 500−700 nm windows, consistent with the fact that these 1D materials comprise closed-cubane species. The discrete 0D closed-cubane clusters **6** and **7** also exhibit low-energy emission, but only **7** exhibits a weak high-energy band at 77 K. This dependence on the temperature and the nature of the sulfur ligand are often observed in cubane species. The microsecond time scale for the τ_e data for **4**−**7** is also fully consistent with what is generally reported for closed-cubane Cu_4I_4 species (Table 1).[24b,34,43a] Some chromaticity data have also been collected (Table 2). All samples emit an overall green emission at 298 K, but complexes **6** and **7** emit red at 77 K, without the maximum shifting very much. This effect is due to a large decrease in the emission bandwidth upon cooling.

Again, the closed-cubane Cu_4I_4-containing species exhibit two emission bands called the high- and low-energy bands.[60−63] A relevant but brief literature overview for the assignments of these two excited states is provided here. The nature of these two emissions was previously addressed by different research teams. Indeed, Ford and his collaborators investigated this subject first using ab initio methods[61a] and, more recently, using density functional theory (DFT) computations.[61b] The outcome of these studies is that these two excited states are either cluster-centered (CC*, i.e., within the Cu_4X_4 skeleton) or halide-to-ligand charge transfer (XLCT). Vega and Saillard reported similar conclusions.[62a] Using DFT calculations, Perruchas, Poilot, and co-workers recently reported on the nature of these low- and high-energy emission bands with a small alteration of the main conclusion.[62b] The low-energy emission ($T_1 \rightarrow S_0$) is due to the combination of a halide-to-copper charge-transfer (XMCT) transition and a copper-centered transition (3d → 4s, 4p, i.e., CC*), which is primarily independent of the nature of the ligand (but not the Cu···Cu distance).[42,61] The high-energy emission ($T_2 \rightarrow S_0$) is assigned to a ^{3}XLCT/^{3}MLCT mixed transition. The simultaneous presence of these two emissions in the spectra is unambiguously due to the large energy gap between T_2 and T_1. Because of the strong structural similarity of the Cu_4I_4 core in the reported materials, these same assignments can, at first glance, be strongly suspected in this work.[63] It is interesting to note that the low-energy emission band is generally the most intense, which is consistent with the fact that this emission arises from the lowest-energy triplet state (i.e., the T_1−S_0 gap is large).

Both clusters **8a** and **8b** are built upon CuI and *i*-Pr_2S (Scheme 3), and their emission and excitation spectra (solid state) at 298 and 77 K are provided in Figure 16. The emission for **8a** exhibits a large band centered at ∼573 (298 K) and ∼532 nm (77 K), becoming narrower at 77 K. This decrease in the bandwidth is due to the common intensity decrease of the "hot bands" (bands arising from vibrationally excited species). Concurrently, cluster **8b** exhibits one band centered at ∼526 nm at 298 K, which shifts to ∼503 nm at 77 K (Figure 16). Moreover, on the high-energy side of this band, a weak signal is also noted at 298 K. This optical fingerprint is, again, consistent with that often encountered for closed-cubane chromophores. Because the structure of **8a** is constituted by two fused closed cubanes, the photophysical properties are anticipated to be similar to those of **8b**. This is indeed the case with some variations. The most noticeable one is the fact that the emission band for **8a** (Cu_8I_8) is slightly red-shifted from that for **8b** (Cu_4I_4), meaning that the emissive state is more stabilized in the former cluster. It is worth noting that both clusters exhibit a double-exponential decay at 77 K with components of similar intensity. One could readily suspect contributions of both high- and low-energy bands, but the relative intensity of the high- and low-energy bands does not match the relative ratio of the two components in the decays. The reasons for this unusual behavior remain unknown.

DOI: 10.1021/acs.inorgchem.5b00327
Inorg. Chem. 2015, 54, 4076−4093

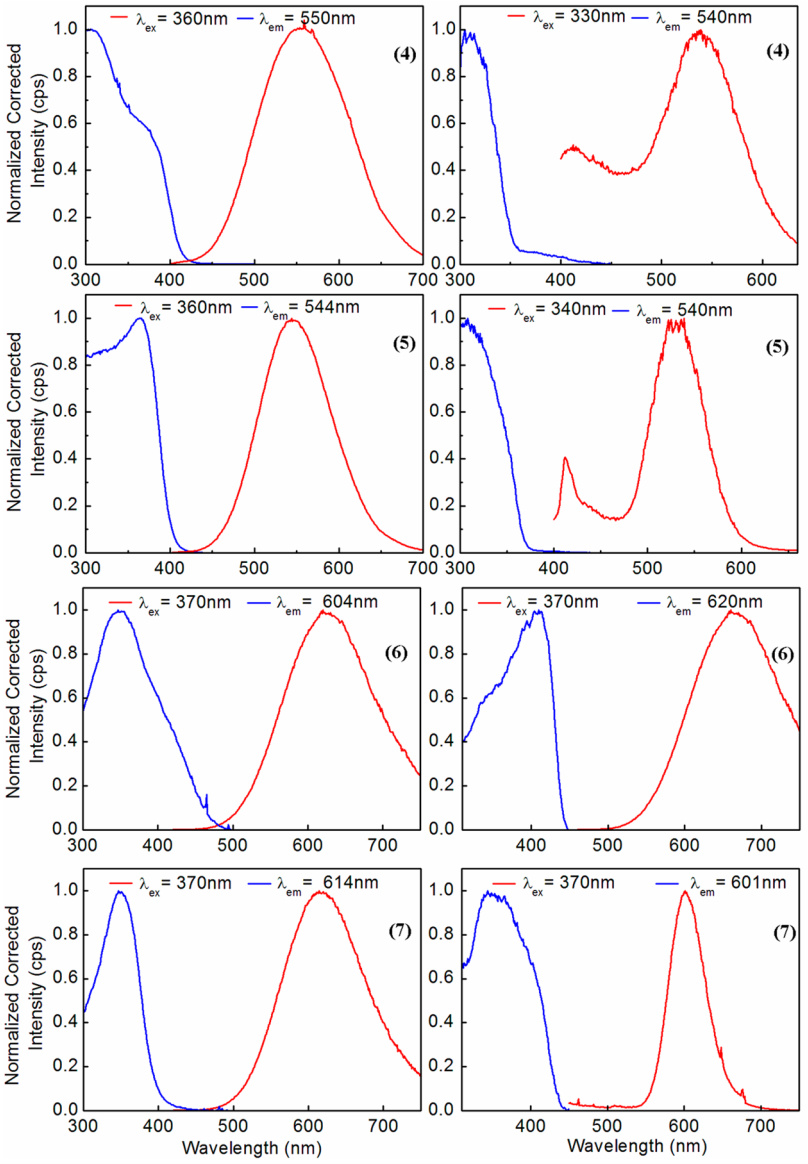

Figure 15. Emission (red) and excitation (blue) spectra of the CPs **4**–**7** at 298 (left) and 77 K (right).

Table 2. Chromaticity Data for 6, 7, 8a, and 8b at 298 and 77 K (the Chromaticity Diagrams are in the SI)

compd	chromaticity at 298 K	chromaticity at 77 K
6	0.45504, 0.52721	0.60386, 0.39491
7	0.37146, 0.58673	0.58396, 0.39356
8a	0.31588, 0.48474	0.37072, 0.40352
8b	0.28353, 0.48455	0.22666, 0.50639

The τ_e values for **8a** are smaller than those for **8b** (Table 1), which indicate that the nonradiative relaxation processes are more efficient for the larger cluster (Cu_8I_8 vs Cu_4I_4). This observation is consistent with the larger size of the cluster giving rise to a larger number of low-frequency vibrational modes contributing to nonradiative pathways. Because of the clear resemblance of the emission maxima, band shapes, and τ_e data for **8a** and **8b** with other closed-cubane-containing materials in the literature and in this work, the assignment for the emissive states can be proposed to be the same at first glance: i.e., the high-energy emission ($T_2 \rightarrow S_0$) is assigned to a ^{3}XLCT/^{3}MLCT mixed transition and the low-energy one ($T_1 \rightarrow S_0$) is ^{3}CC*.[61−63] Hou and co-workers also investigated this rare motif (Cu_8I_8) using dabco as the ligand.[57] They reported similar photophysical properties, and a narrow emission band centered at ∼580 nm was assigned to ^{3}CC* as well;[57] see also the work on $[Cu_8I_8(4\text{-dpda})_6]_n$ [4-dpda = 4-(diphenylphosphino)-*N*,*N*-dimethylaniline], where an in-depth photophysical study has been reported in ref 57d. However, DFT and time-dependent DFT (TDDFT) suggest a slightly different scenario below.

The emission spectra for the bromine-containing polymer **9** at 77 and 298 K exhibit a band maximum in the vicinity of 440 nm (Figure 17). Some vibronic features are also noted, and the emission band shape is reminiscent of that previously reported on similar rhomboid motifs ($S_2Cu(\mu\text{-}X)_2CuS_2$; X = Br, I).[64] On the basis of the microsecond time scale for the τ_e values (Table 1), these emissions also arise from a triplet manifold. A ^{3}M/XLCT assignment for these emissions can reasonably be made based on previous extended Hückel molecular orbital (MO) calculations on related bimetallic species $Ag_2(\mu\text{-}X)_2(dmb)_2$ (X = Cl, Br, I; dmb = 1,8-diisocyanomenthane).[65]

DOI: 10.1021/acs.inorgchem.5b00327
Inorg. Chem. 2015, 54, 4076−4093

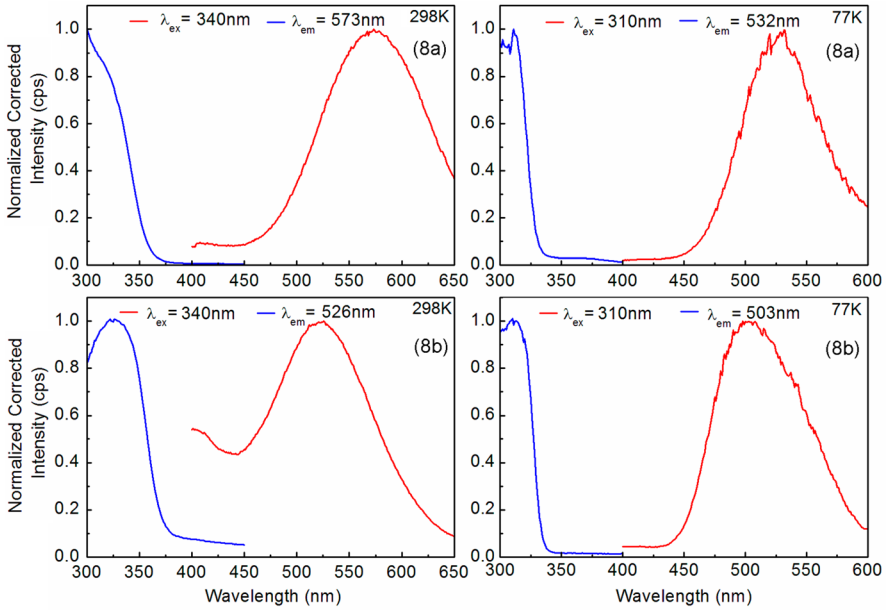

Figure 16. Emission (red) and excitation (blue) spectra of 0D clusters **8a** and **8b** at 298 (left) and 77 K (right).

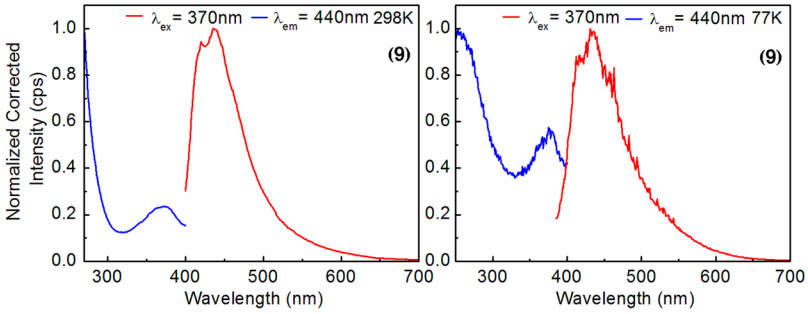

Figure 17. Emission (red) and excitation (blue) spectra of the polymer **9** at 298 K (left) and 77 K (right).

11. Time-Resolved Emission Spectroscopy (TRES). Again, Table 1 reports τ_e values in the microsecond time scale that are typical for closed-cubane species[35,43,64] and were also corroborated by TRES. Attempts to detect two bands with slightly different maxima and τ_e values, if any, failed, particularly for the sought high-energy side of the emission bands of **8a** and **8b** (Figure 18; the 2D and 3D maps are given in the SI).

12. Absorption Spectra of 8a and Computational Study. The solid-state absorption spectra of **8a** at 298 and 77 K exhibit strong absorption bands in the 300−425 nm range and one weaker one at ∼470 nm (Figure 19). These features can reasonably be assigned to spin-allowed and spin-forbidden transitions, respectively, based on the position of the excitation (blue) and emission (red) bands.

This interpretation was confirmed using DFT (B3LYP) and TDDFT calculations addressing the nature of the excited states at the same time (Figure 19 and Figure S7 and Table S9 in the SI). To the best of our knowledge, no computational study for the Cu_8I_8 chromophore exists. The representations of the frontier MOs of **8a** exhibit atomic contributions expectedly distributed over the Cu, I, and S atoms but dominantly located on the Cu_8I_8 cluster (Table 3). The five first spin-allowed calculated electronic transitions (TDDFT) place the low-energy absorption bands in the 300 nm range. This result supports the assignment for the absorption features in the vicinity of 300 nm being $S_0 \rightarrow S_n$ transitions. Moreover, all five

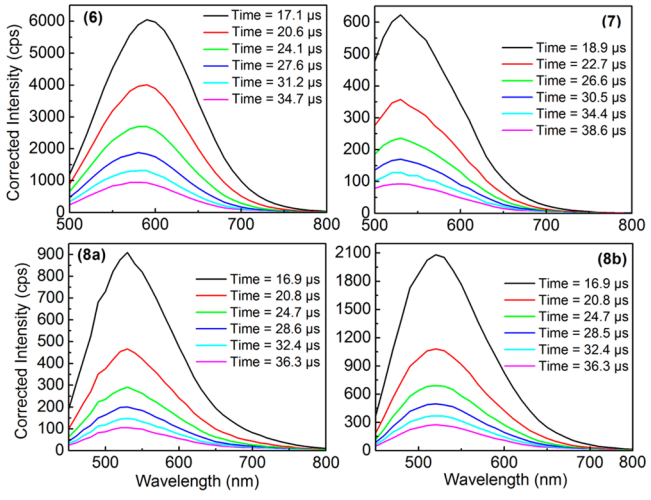

Figure 18. Sliced TRES recorded in the solid state for **6**, **7**, **8a**, and **8b** at 298 K. The 2D and 3D maps are given in the SI (Figure S11).

first calculated singlet−singlet electronic transitions exhibit major contributions of the type highest occupied molecular orbital (HOMO, H−1, H−2, H−3, or H−4) → lowest unoccupied molecular orbital (LUMO). On the basis of the data of Table 4, the atomic contributions for each individual

DOI: 10.1021/acs.inorgchem.5b00327
Inorg. Chem. 2015, 54, 4076−4093

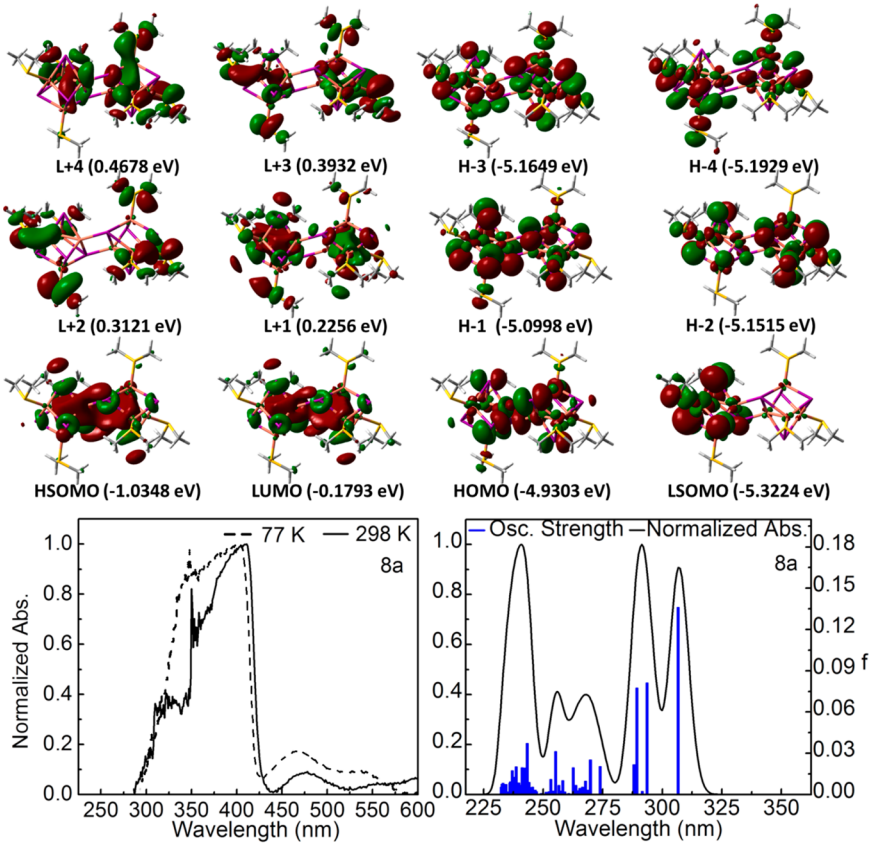

Figure 19. (top) representation of the frontier MOs of the Cu_8I_8 fragment in **8a** (the input file was built using the X-ray data at 173 K, except that the ligands were replaced by terminal SMe_2 ligands to save computation time. (bottom) Left: Absorption spectra of **8a** at 298 (black) and 77 K (broken gray line). Right: First 80 computed electronic transitions (TDDFT; blue bar graph; *f* = computed oscillator strength). The black line is generated by assigning a thickness of 500 cm^{-1} to each bar.

Table 3. Atomic Distributions of the Frontier MOs for Cu_8I_8

	H−4	H−3	H−2	H−1	HOMO	LUMO	L+1	L+2	L+3	L+4
Cu_8I_8	78.0	82.5	81.3	85.2	93.2	92.5	89.8	70.6	63.5	58.0
SMe_2	21.2	17.5	18.7	14.8	6.1	7.5	10.2	29.4	35.5	42.0

Table 4. Calculated Position, Oscillator Strength (*f*), and Major Contributions of the First Five Singlet−Singlet Electronic Transitions for the Cu_8I_8 Chromophore[a]

λ, nm	*f*	major contributions (%)
306.6	0.1359	HOMO → LUMO (95)
293.6	0.0810	H−1 → LUMO (87)
291.5	0.0021	H−2 → LUMO (81)
289.3	0.0773	H−4 → LUMO (10), H−3 → LUMO (74)
288.1	0.0215	H−4 → LUMO (71), H−3 → LUMO (10)

[a]The first 80 computed electronic transitions are given in the SI (Table S8).

MO involved are concentrated on the Cu_8I_8 cluster (80−90%). So, all of these five transitions are mostly occurring within the Cu_8I_8 cluster as for the closed Cu_4I_4 cubanes (i.e., CC*), but a weak ligand-to-metal charge transfer (LMCT) process is also noted for the computed upper energy transitions (H−1, H−2, H−3, and H−4 → LUMO).

It is worth noting that the computations of the representations of the high and low semioccupied MOs, HSOMO and LSOMO, respectively (Figure 19), are particularly interesting. The atomic contributions of HSOMO and LUMO are very similar, which is often the case. However, the atomic contributions of LSOMO are drastically concentrated over one cubane, whereas the filled MOs (HOMO, H−1, H−2, H−3, and H−4) exhibit atomic distributions fairly well distributed over both cubanes (details are given in Figure S8 in the SI). This means that the lowest-energy triplet state is not a typical ^{3}CC* but rather a cluster-to-cluster charge transfer (^{3}CCCT*), which would thus explain why the emission band of the Cu_8I_8 chromophore is red-shifted with respect to that of the classic Cu_4I_4 closed cubane. This interesting result is completely new for this class of cluster.

CONCLUSION

This exhaustive study on the apparently simple coordination chemistry of CuI with aliphatic thioether ligands RSR, which was first documented in the 1970s, is far more complicated than the simple formation of a given CuI·RSR adduct. An impressive structural richness is encountered, which ranges from tetranuclear molecular clusters of the closed-cubane-type $[(RSR)_4\{Cu_4(\mu_3\text{-}I)_4\}]$ to the octanuclear cluster **8a**. The cluster nuclearity and dimensionality seem to be dictated by steric crowding on the alkyl substituent of the RSR ligand because with smaller alkyl groups (Me and Et) preferentially

DOI: 10.1021/acs.inorgchem.5b00327
Inorg. Chem. 2015, 54, 4076−4093

1D CPs with bridging μ_2-RSR ligands are preferentially assembled. However, the cluster size of the $(CuI)_n$ SBU is variable, being a dinuclear rhomboid as in **1** or a closed cubane as encountered in **4**, $[(Et_2S)_3\{Cu_4(\mu_3\text{-}I)_4\}]_n$, and **5**. In addition, the solvent choice has a crucial impact on the resulting architecture of the thioether adducts. Changing from a nonpolar reaction media like *n*-hexane or *n*-heptane to MeCN can lead to different polymer compositions because MeCN can act as a ligand. This has been demonstrated from the reaction of CuI with MeSEt, leading to the 1D CP **3** or **4** using MeCN or *n*-heptane, respectively. A second example is the reaction product of Me_2S, with CuI producing **1** or the 2D MOF **2** containing "flower-basket" Cu_4I_4 units. The volatility of Me_2S probably accounts for the solid-state transformation of the CP **1** to **2**. However, this solvent impact cannot be generalized because the reaction product of CuI with MeSPr, EtSPr, and $S(i\text{-}Pr)_2$ is independent of the reaction medium.

Our investigation has, furthermore, demonstrated that the nature of the halide ligand also plays an important role. As was previously observed, the architecture and topology of the CuBr·RSR adducts is quite different compared to their CuI analogues, as evidenced by the structural characterization of the 2D material **9** and the 1D CP **10**. The conversion of **10** to a 2D MOF **11** incorporating pentanuclear $[(Cu_5(\mu_4\text{-}Br)(\mu_2\text{-}Br)]$ SBUs in MeCN nicely demonstrates that, also in the case of CuBr, the solvent polarity may play a key factor. An in-depth crystallographic examination of some representative compounds at variable temperature has also shed some light on the evolution of the metric parameters as a function of the temperature.

TGA indicates a lower thermal stability [65 °C < T_{dec} (at 5% mass loss) < 121 °C] than those for other closed-cubane $Cu_4I_4S_x$-containing species and related materials (T_{dec} > 150 °C) assembled by dithioether ligands.[35,43,55,64] Speculatively, this behavior could be associated with the more volatile character of the RSR ligands. The encountered motifs, open- ("flower-basket"), closed-, and fused-cubane species, are found to be luminescent at 77 and 298 K and exhibit τ_e values in the microsecond time scale. This observation is not surprising because this is generally the case for such motifs. The Cu_8I_8-containing chromophore was studied for its photophysical properties for the first time (to the best of our knowledge), and the computational conclusion suggests a new type of emissive excited state: ^{3}CCCT*. The generalization of this interesting new feature can only be achieved with a larger number of examples. The obvious problem is that this motif is extremely rare, and the selective synthesis of a motif versus another remains completely illusive.

EXPERIMENTAL SECTION

Materials. CuI and CuBr were purchased from Acros and the thiols from Alfa Aesar and Aldrich. The CPs **1** and **5** were prepared as previously reported in the literature.[43b,45]

Preparation of Polymer 2. CuI (0.282 g, 2 mmol) was dissolved in MeCN (10 mL), and then Me_2S was added in excess (0.73 mL, 10 mmol). The resulting clear solution was stirred for 2 h, and the Schlenk tube was placed inside a refrigerator (5 °C), where colorless crystals of **2** crystallized overnight. A second crop was isolated after the filtered solution was kept in a freezer at −20 °C. Overall yield: 75%. Anal. Calcd for $C_6H_{18}Cu_4I_4S_3$ (948.21): C, 7.60; H, 1.91; S, 10.15. Found: C, 7.94; H, 2.15; S, 10.51.

Preparation of Polymer 3. CuI (0.282 g, 2 mmol) was dissolved in MeCN (10 mL), and MeSEt was added (0.53 mL, 6 mmol). The resulting clear solution was stirred for 2 h, and the Schlenk tube was placed inside a refrigerator (5 °C), where colorless crystals of **3** crystallized overnight. A second crop was isolated after the filtered solution was kept in freezer at −20 °C. Overall yield: 68%. This compound was too unstable (the ligand evaporated) to obtain satisfactory elemental analysis.

Preparation of Polymer 4. CuI (0.384 g, 2 mmol) was dissolved in neat MeSEt (2 mL) (exothermic reaction), and the resulting yellow viscous solution was stirred for a further 2 h in a Schlenk tube. *n*-Heptane (10 mL) was added slowly to form a layer. In the course of several hours, colorless crystals of **4** appeared. The Schlenk tube was placed inside a refrigerator (5 °C) overnight to complete the crystallization process. A second crop of this air-stable compound was isolated after the filtered solution was kept in a freezer at −20 °C. Overall yield: 76%. Anal. Calcd for $C_9H_{24}Cu_4I_4S_3$ (990.29): C, 10.91; H, 2.44; S, 9.71. Found: C, 11.06; H, 2.50; S, 9.52.

Preparation of Cluster 6. CuI (0.384 g, 2 mmol) was dissolved in neat EtSPr (2 mL) (exothermic reaction), and the resulting yellow viscous solution was stirred for a further 2 h in a Schlenk tube. *n*-Heptane (10 mL) was added slowly to form a layer. In the course of several hours, colorless crystals of **6** started to grow. The Schlenk tube was placed inside a refrigerator to complete the crystallization process. Overall yield: 73%. Anal. Calcd for $C_{20}H_{48}Cu_4I_4S_4$ (1178.67): C, 20.38; H, 4.10; S, 10.88. Found: C, 20.06; H, 3.95; S, 10.56.

Preparation of Cluster 7. CuI (0.573 g, 3 mmol) was dissolved in neat SPr_2 (3 mL), and the resulting yellow viscous solution was stirred for a further 2 h in a Schlenk tube. *n*-Hexane (15 mL) was added slowly to form a layer. The Schlenk tube was placed inside a refrigerator (5 °C), where colorless crystals of **7** started to grow. Overall yield: 76%. No satisfying elemental analysis could be obtained from the waxy solid formed at room temperature.

Preparation of Cluster 8a. CuI (0.573 g, 3 mmol) was dissolved in MeCN (15 mL), and $S(i\text{-}Pr)_2$ was added in excess (1.160 mL, 8 mmol). The resulting clear solution was stirred for 2 h. The volume was reduced to 10 mL, and the Schlenk tube was placed inside a refrigerator (5 °C), where colorless crystals of **8a** crystallized overnight. Overall yield: 67%. Anal. Calcd for $C_{36}H_{84}Cu_8I_8S_6$ (2233.06): C, 19.36; H, 3.79; S, 8.61. Found: C, 19.57; H, 3.90; S, 8.76.

Preparation of Polymer 9. CuBr (1.435 g, 10 mmol) was dissolved in neat MeSEt (5 mL), and the resulting brown-yellow solution was stirred for a further 5 h in a Schlenk tube. *n*-Heptane (15 mL) was layered in three portions. During the addition of the last portion, precipitation of a small amount of a colorless solid was noticed. The Schlenk tube was placed inside a refrigerator (5 °C), where large slightly brownish crystals of **9** crystallized overnight. A second crop was also isolated after the filtered solution was kept in freezer at −20 °C. Overall yield: 68%. Anal. Calcd for $C_{12}H_{32}Br_4Cu_4S_4$ (878.45): C, 16.41; H, 3.67; S, 14.60. Found: C, 16.26; H, 3.25; S, 14.22.

Preparation of Polymer 10. CuBr (0.715 g, 5 mmol) was dissolved in neat MeSPr (4 mL), and the resulting brown-yellow solution was stirred for a further 5 h in a Schlenk tube. *n*-Heptane (15 mL) was layered in three portions. During the addition of the last portion, precipitation of a small amount of a colorless solid was noticed. The Schlenk tube was placed inside a refrigerator, where large slightly brownish crystals of **10** crystallized overnight. Overall yield: 70%. Anal. Calcd for $C_{12}H_{30}Br_3Cu_3S_3$ (700.92): C, 20.56; H, 4.31; S, 13.72. Found: C, 20.26; H, 4.15; S, 13.40.

Instruments. The UV−vis spectra were recorded on a Varian Cary 50 spectrophotometer at 298 and 77 K using a grazing-angle transmittance apparatus and a homemade 77 K sample holder. Steady-state fluorescence and excitation spectra were acquired on either a Fluorolog SPEX 1680 equipped with double monochromators for both excitation and emission arms or an Edinburgh Instruments FLS980 phosphorimeter equipped with single monochromators. All samples were crushed, and the steady-state fluorescence spectra were recorded using a capillary. Those spectra were corrected for instrument response. Phosphorescence lifetime measurements were performed and emission lifetimes measured on a LS100 apparatus from PTI or with an Edinburgh Instruments FLS980 phosphorimeter

DOI: 10.1021/acs.inorgchem.5b00327
Inorg. Chem. 2015, 54, 4076−4093

equipped with a "flash" pulsed lamp. The pulse frequency was adjusted from 1 to 100 Hz. All lifetime values were obtained from deconvolution and distribution lifetime analysis. TRES was performed with an Edinburgh Instruments FLS980 phosphorimeter equipped with a "flash" xenon pulsed lamp. The latter instrument was also used to measure the chromaticity. The TGA traces were acquired on a PerkinElmer TGA 7 apparatus in the temperature range between 20 and 950 °C at 10 °C/min under a nitrogen atmosphere. The figures have been treated with *Origin 8* except the TRES images, which have been drawn by *Origin 9.1*.

Computational. All DFT, for singlet and triplet states, as well as TDDFT calculations were performed with *Gaussian 09* at the Université de Sherbrooke with the Mammouth supercomputer supported by Le Réseau Québécois De Calculs Hautes Performances. The CIF files from the X-ray structures have been used to optimize the structures for calculations.[66] The DFT and TDDFT calculations were carried out using the B3LYP method.[67−75] VDZ (valence double ζ) with SBKJC effective core potentials were used for all Cu and I atoms; a 6-31g* basis set was used for the C, H, and S atoms.[76] The calculated absorption spectra were obtained from *GaussSum 2.1*.[77]

X-ray Crystallography. Colorless single crystals of **2**−**4**, **6**, **7**, **9**, and **10** were mounted on a Nonius Kappa Apex-II CCD diffractometer equipped with a nitrogen jet stream low-temperature system (Oxford Cryosystems). Crystals of **5** and **8a** were mounted on Bruker APEXII and Xcalibur Sapphire3 diffractometers, respectively. Diffraction data (monochromated Mo Kα radiation, λ = 0.71073 Å) were recorded for **5** and **9** at five temperatures (115, 155, 195, 235, and 275 K), whereas for **7**, the correct variable-temperature data could be collected only at the four lower temperatures; a very poor and untreatable diffraction pattern was obtained at 275 K for **7**. Data for **8a** were measured at 173 K and those for **2**−**4**, **6**, and **10** at 115 K. Data were reduced with Denzo and Scalepack[78] (**2**, **4**, **6**, **7**, and **9**), *SAINT*[79] (**3** and **10**), and *SORTAV* (**5**) with empirical multiscan absorption corrections of Blessing[80] for **2**, **6**, **7**, and **9**, *SADABS*[79] for **3**, **5**, and **10**, and *CrysAlisPro*[81] for **8a**. The structures were solved by direct methods with the *SHELXS97*[82] (**3**, **4**, **8a**, and **10**) and *SIR92*[83] (**2**, **5**−**7**, and **9**) programs. Refinements of all structures were carried out by full-matrix least squares on F^2 using the *SHELXL97* program.[82] In the 0D molecular structure of **6**, one of the two independent thioether ligands (based of the S2 atom in Figure 5) is disordered. The statistical occupancies were refined to 0.7 for ligand A and to 0.3 for minor ligand B. The latter one occupies a very close position without any chemical meaning. All non-H atoms were refined with anisotropic thermal parameters. The H atoms were placed in calculated positions and included in the final refinement in a riding model, with the isotropic temperature parameters set to $U_{iso}(H) = 1.2U_{eq}$ for methylene CH_2 and aryl CH C atoms and to $1.5U_{eq}$ for methyl CH_3 groups. Crystal data, data collection, and structure refinement of all compounds are presented in Tables S4−S7 in the SI.

Crystallographic data (excluding structure factors) have been deposited with the Cambridge Crystallographic Data Centre. The CIF files for the X-ray structures presented in this publication have the following CCDC numbers: 1047394 for **2** at 115 K, 1047395 for **3**, 1047396 for **4**, 1047397 for **6**, 1047398 for **8a** at 173 K, 1047399 for **10**, 1047400 for **5** at 115 K, 1047401 for **5** at 155 K, 1047402 for **5** at 195 K, 1047403 for **5** at 235 K, 1047404 for **5** at 275 K, 1047405 for **7** at 115 K, 1047406 for **7** at 155 K, 1047407 for **7** at 195 K, 1047408 for **7** at 235 K, 1047409 for **9** at 115 K, 1047410 for **9** at 155 K, 1047411 for **9** at 195 K, 1047412 for **9** at 235 K, and 1047413 for **9** at 275 K. These data may be obtained free of charge from the Cambridge Crystallographic Data Center through www.ccdc.cam.ac.uk/data_request/cif.

■ ASSOCIATED CONTENT

Supporting Information

Crystallographic data in CIF format, summary of X-ray data collection and refinement of compounds **3**−**8a**, **9**, and **10**, temperature-dependent cluster volumes for **5**, **7**, and **9**, relative distribution of DFT-calculated frontier MOs of **8a**, electronic transition energy, oscillator strength (f), and major contributions of the first 80 singlet−singlet electronic transitions TDDFT-calculated for **8a** at 173 K, chromaticity of **6**, **8a**, and **8b** at 298 and 77 K, and TRES maps recorded in the solid state for **6**, **7**, **8a**, and **8b** at 298 K. This material is available free of charge via the Internet at http://pubs.acs.org.

■ AUTHOR INFORMATION

Corresponding Authors

*E-mail: michael.knorr@univ-fcomte.fr.
*E-mail: marek.kubicki@u-bourgogne.fr.
*E-mail: Pierre.Harvey@USherbrooke.ca.

Notes

The authors declare no competing financial interest.

■ ACKNOWLEDGMENTS

This work was supported by the CNRS, the Natural Sciences and Engineering Research Council of Canada, and the Centre Québécois des Matériaux Fonctionnels.

■ REFERENCES

(1) (a) Ahna, H. D. D.; Hardt, H. D. *Z. Anorg. Allg. Chem.* **1972**, *387*, 61−71. (b) Hardt, H. D.; Pierre, A. *Z. Anorg. Allg. Chem.* **1973**, *402*, 107−112. (c) Eitel, E.; Oelkrug, D.; Hiller, W.; Strähle, J. *Z. Naturforsch.* **1980**, *35B*, 1247−1253.

(2) (a) Dyason, J. C.; Healy, P. C.; Engelhardt, L. M.; Pakawatchai, C.; Patrick, V. A.; Raston, C. L.; White, A. H. *J. Chem. Soc., Dalton Trans.* **1985**, 831−838. (b) Graham, A. J.; Healy, P. C.; Kildea, J. D.; White, A. H. *Aust. J. Chem.* **1989**, *42*, 177−184. (c) Healy, P. C.; Kildea, J. D.; Skelton, B. W.; White, A. H. *Aust. J. Chem.* **1989**, *42*, 79−91.

(3) (a) Goel, R. G.; Beauchamp, A. L. *Inorg. Chem.* **1983**, *22*, 395−400. (b) Kitagawa, H.; Ozawa, Y.; Toriumi, K. *Chem. Commun.* **2010**, 6302−6304.

(4) (a) Lapprand, A.; Dutartre, M.; Khiri, N. M.; Levert, E.; Fortin, D.; Rousselin, Y.; Soldera, A.; Jugé, S.; Harvey, P. D. *Inorg. Chem.* **2013**, *52*, 7958−7967. (b) Emerson, E. W.; Cain, M. F.; Sanderson, M. D.; Knarr, C. B.; Glueck, D. S.; Ahern, J. C.; Patterson, H. E.; Rheingold, A. L. *Inorg. Chim. Acta* **2015**, *427*, 168−172.

(5) Graham, P. M.; Pike, R. D.; Sabat, M.; Bailey, R. D.; Pennington, W. T. *Inorg. Chem.* **2000**, *39*, 5121−5132.

(6) (a) Gschwind, F.; Sereda, O.; Fromm, K. M. *Inorg. Chem.* **2009**, *48*, 10535−10547. (b) Zink, D. M.; Bächle, M.; Baumann, T.; Nieger, M.; Kühn, M.; Wang, C.; Klopper, W.; Monkowius, U.; Hofbeck, T.; Yersin, H.; Bräse, S. *Inorg. Chem.* **2013**, *52*, 2292−2305. (c) Näther, C.; Wriedt, M.; Jeß, I. *Z. Anorg, Allg. Chem.* **2002**, *628*, 394−400. (d) Pospisil, J.; Jess, I.; Näther, C.; Necas, M.; Taborsky, P. *New J. Chem.* **2011**, *35*, 861−864. (e) Xin, B.-J.; Li, Y.; Zeng, G.; Peng, Y.; Li, G.-H.; Shi, Z.; Feng, S.-H. *Z. Anorg. Allg. Chem.* **2013**, *639*, 611−617. (f) Liu, S.-S.; Yuan, S.; Hu, T.-P.; Sun, D. *Z. Anorg. Allg. Chem.* **2014**, *640*, 2030−2034. (g) Tsuge, K. *Chem. Lett.* **2013**, *640*, 204−208.

(7) (a) Hakansson, M.; Jagner, S. *J. Organomet. Chem.* **1990**, *397*, 383−393. (b) Haakansson, M.; Jagner, S.; Clot, E.; Eisenstein, O. *Inorg. Chem.* **1992**, *31*, 5389−5394. For the coordination of phenyl propargyl and allyl methyl sulfide on CuCl and CuBr, see: Kokoli, T.; Olsson, S.; Bjoremark, P. M.; Persson, S.; Hakansson, M. *J. Organomet. Chem.* **2013**, *724*, 17−22.

(8) Streciwilk, W.; Hackenberg, F.; Müller-Bunz, H.; Tacke, M. *Polyhedron* **2014**, *80*, 3−9.

(9) (a) Olbrich, F.; Schmidt, G.; Behrens, U.; Weiss, E. *J. Organomet. Chem.* **1991**, *418*, 421−429. (b) Olbrich, F.; Kopf, J.; Weiss, E. *J. Organomet. Chem.* **1993**, *456*, 293−298.

(10) Fox, B. J.; Sun, Q. Y.; DiPasquale, A. G.; Fox, A. R.; Rheingold, A. L.; Figueroa, J. S. *Inorg. Chem.* **2008**, *47*, 9010−9020.

(11) Kaim, W.; Rall, J. *Angew. Chem., Int. Ed. Engl.* **1996**, *35*, 43−60.

DOI: 10.1021/acs.inorgchem.5b00327
Inorg. Chem. 2015, 54, 4076−4093

(12) Holm, R. H.; Kennepohl, P.; Solomon, E. I. *Chem. Rev.* **1996**, *96*, 2239−2314.
(13) Rorabacher, D. B. *Chem. Rev.* **2004**, *104*, 651−698.
(14) (a) Solomon, E. I.; Clendening, P. J.; Gray, H. B.; Grunthaner, F. J. *J. Am. Chem. Soc.* **1975**, *97*, 3878−3879. (b) Solomon, E. I.; Heppner, D. E.; Johnston, E. M.; Ginsbach, J. W.; Cirera, J.; Qayyum, M.; Kieber-Emmons, M. T.; Kjaergaard, C. H.; Hadt, R. G.; Tian, L. *Chem. Rev.* **2014**, *114*, 3659−3853. (c) Penfield, K. W.; Gay, R. R.; Himmelwright, R. S.; Eickman, N. C.; Norris, V. A.; Freeman, H. C.; Solomon, E. I. *J. Am. Chem. Soc.* **1981**, *103*, 4382−4388.
(15) Colman, P. M.; Freeman, H. C.; Guss, J. M.; Murata, M.; Norris, V. A.; Ramshaw, J. A. M.; Venkatapp, M. P. *Nature* **1978**, *272*, 319−324.
(16) Gray, H. B.; Malmström, B. G. *Comments Inorg. Chem.* **1983**, *2*, 203−209.
(17) Sykes, A. G. *Chem. Soc. Rev.* **1985**, *14*, 283−315.
(18) Baker, E. N.; Garrick, P. M. *J. Chem. Soc., Dalton Trans.* **1978**, 416−418.
(19) Warner, L. G.; Ottersen, T.; Seff, K. *Inorg. Chem.* **1974**, *13*, 2819−2826. (b) Karlin, K. D.; Yandell, J. K. *Inorg. Chem.* **1984**, *23*, 1184−1188.
(20) Guckert, J. A.; Lowery, M. D.; Solomon, E. I. *J. Am. Chem. Soc.* **1995**, *117*, 2817−2844.
(21) Louvain, N.; Mercier, N.; Kurmoo, M. *Eur. J. Inorg. Chem.* **2008**, 1654−1160.
(22) (a) Rostovshchikova, T. N.; Smirnov, V. V.; Kharitonov, D. N.; Rybakov, V. B. *Russ. Chem. Bull.* **1997**, *46*, 1736−1740. (b) Rostovshchikova, T. N.; Smirnov, V. V.; Kokorin, A. I. *J. Mol. Catal. A: Chem.* **1998**, *129*, 141−151.
(23) (a) House, H. O.; Chu, C.-Y.; Wilkins, J. M.; Umen, M. J. *J. Org. Chem.* **1975**, *40*, 1460−1469. (b) Park, I.-H.; So, M.-S.; Park, K.-H. *Bull. Korean Chem. Soc.* **2007**, *28*, 1515−1518.
(24) (a) Killarney, J. P.; McKinnon, M.; Murphy, C.; Henline, K. M.; Wang, C.; Pike, R. D.; Patterson, H. H. *Inorg. Chem. Commun.* **2014**, *40*, 18−21. (b) Henline, K. M.; Wang, C.; Pike, R. D.; Ahern, J. C.; Sousa, B.; Patterson, H. H.; Kerr, A. T.; Cahill, C. L. *Cryst. Growth Des.* **2014**, *14*, 1449−1458.
(25) Pearson, R. G. *Inorg. Chim. Acta* **1995**, *240*, 93−98.
(26) Cohen, B.; Ou, C. C.; Lalancette, R. A.; Borowski, W.; Potenza, J. A.; Schugar, H. J. *Inorg. Chem.* **1979**, *18*, 217−298.
(27) Olmstead, M. M.; Musker, W. K.; Ter Haar, L. W.; Hatfield, W. E. *J. Am. Chem. Soc.* **1982**, *104*, 6627−6631.
(28) Ainscough, E. W.; Brodie, A. M.; Husbands, J. M.; Gainsford, G. J.; Gabe, E. J.; Curtis, N. F. *J. Chem. Soc., Dalton Trans.* **1985**, 151−158.
(29) Guy, J. T., Jr.; Cooper, J. C.; Gilardi, R. D.; Flippen-Anderson, J. L.; George, C. F., Jr. *Inorg. Chem.* **1988**, *27*, 635−638.
(30) (a) Olbrich, F.; Mälger, H.; Klar, G. *Transition Met. Chem.* **1992**, *17*, 525−529. (b) Noren, B.; Oskarsson, A. *Acta Chem. Scand.* **1987**, *A41*, 12−17.
(31) (a) Barnes, J. C.; Paton, J. D. *Acta Crystallogr., Sect. B* **1982**, *38*, 3091−3093. (b) Barnes, J. C.; Paton, J. D.; McKissock, A. *Acta Crystallogr., Sect. C* **1983**, *39*, 547−550. (c) Cheng, J.-K.; Yao, J.-G.; Zhang, J.; Li, Z.-J.; Cai, Z.-W.; Zhang, X.-Y.; Chen, Z.-N.; Chen, Y.-B.; Kang, Y.; Qin, Y.-Y.; Wen, Y.-H. *J. Am. Chem. Soc.* **2004**, *126*, 7796−7797.
(32) (a) Blake, A. J.; Brooks, N. R.; Champness, N. R.; Cooke, P. A.; Deveson, A. M.; Fenske, D.; Hubberstey, P.; Li, W.-S.; Schröder, M. *J. Chem. Soc., Dalton Trans.* **1999**, 2103−2110. (b) Peng, R.; Li, M.; Li, D. *Coord. Chem. Rev.* **2010**, *254*, 1−18.
(33) (a) Knorr, M.; Guyon, F. Luminescent oligomeric and polymeric copper coordination compounds assembled by thioether ligands. In *Macromolecules containing metal and metal-like elements: Photophysics and photochemistry of metal-containing polymers*; Aziz, A. S. A.-E., Carraher, C. E., Harvey, P. D., Pittmann, C. U., Zeldin, M., Eds.; John Wiley & Sons: New York, 2010; Vol. *10*, pp 89−158. (b) Harvey, P. D.; Knorr, M. *Macromol. Rapid Commun.* **2010**, *31*, 808−826. (c) Harvey, P. D.; Knorr, M. *J. Cluster Sci.* **2015**, *26*, 411−459.
(34) Xue, X.; Wang, X.-S.; Xiong, R.-G.; You, X.-Z.; Abrahams, B. F.; Che, C.-M.; Ju, H.-X. *Angew. Chem., Int. Ed.* **2002**, *41*, 2944−2946.
(35) (a) Knorr, M.; Guyon, F.; Khatyr, A.; Däschlein, C.; Strohmann, C.; Aly, S. M.; Abd-El-Aziz, A. S.; Fortin, D.; Harvey, P. D. *Dalton Trans.* **2009**, 948−955. (b) Aly, S.; Pam, A.; Khatyr, A.; Knorr, M.; Rousselin, Y.; Kubicki, M. M.; Bauer, J. O.; Strohmann, C. M.; Harvey, P. D. *J. Inorg. Organomet. Polym.* **2014**, *24*, 190−200.
(36) Siemeling, U.; Vorfeld, U.; Neumann, B.; Stammler, H.-G. *Chem. Commun.* **1997**, 1723−1724.
(37) Poblet, J.-M.; Benard, M. *Chem. Commun.* **1998**, 1179−1180.
(38) Che, C.-M.; Mao, Z.; Miskowski, V. M.; Tse, M.-C.; Chan, C.-K.; Cheung, K.-K.; Phillips, D. L.; Leung, K.-H. *Angew. Chem., Int. Ed.* **2000**, *39*, 4084−4088.
(39) Hermann, H. L.; Boche, G.; Schwerdtfeger, P. *Chem.—Eur. J.* **2001**, *7*, 5333−5342.
(40) Zheng, S.-L.; Messerschmidt, M.; Coppens, P. *Angew. Chem., Int. Ed.* **2005**, *44*, 4614−4617.
(41) San Filippo, J.; Zyontz, L. E.; Potenza, J. *Inorg. Chem.* **1975**, *14*, 1667−1671.
(42) (a) Ford, P. C. *Coord. Chem. Rev.* **1994**, *132*, 129−140. (b) Vitale, M.; Ford, P. C. *Coord. Chem. Rev.* **2001**, *219−221*, 3625−3648.
(43) (a) Knorr, M.; Pam, A.; Khatyr, A.; Strohmann, C.; Kubicki, M. M.; Rousselin, Y.; Aly, S. M.; Fortin, D.; Harvey, P. D. *Inorg. Chem.* **2010**, *49*, 5834. (b) Lapprand, A.; Bonnot, A.; Knorr, M.; Rousselin, Y.; Kubicki, M. M.; Fortin, D.; Harvey, P. D. *Chem. Commun.* **2013**, *49*, 8848−8850.
(44) Lenders, B.; Grove, D. M.; Van Koten, G.; Smeets, W. J. J.; Van der Sluis, P.; Spek, A. L. *Organometallics* **1991**, *10*, 786−791.
(45) Mälger, H.; Olbrich, F.; Kopf, J.; Abeln, D.; Weiss, E. *Z. Naturforsch. B* **1992**, *47*, 12−17.
(46) (a) Zhou, J.; Bian, G.-Q.; Dai, J.; Zhang, Y.; Zhu, Q.-Y.; Lu, W. *Inorg. Chem.* **2006**, *45*, 8486−8488. (b) Crystal data for **2** at 115 K: $C_6H_{18}Cu_4I_4S_3$; M_r = 948.14; colorless prism 0.30 × 0.10 × 0.10 mm; orthorhombic *Cmca*; a = 12.858(5) Å, b = 29.651(5) Å, c = 10.705(5) Å; V = 4081(3) Å^3; Z = 8; d_{calc}= 3.086 g/cm^3; F_{000} = 3440; μ = 10.451 mm^{-1}; abs corr T_{min} = 0.1235, T_{max} = 0.3507; independent reflections 2406; R = 0.0558; R_w = 0.1248, GoF = 1.229..
(47) (a) Healy, P. C.; Pakawatchai, C.; Raston, C. L.; Skelton, B. W.; White, A. H. *J. Chem. Soc., Dalton Trans.* **1983**, 1905. (b) Manbeck, G. F.; Brennessel, W. W.; Evans, C. M.; Eisenberg, R. *Inorg. Chem.* **2010**, *49*, 2834−2843.
(48) For a 1D CP containing stair-step Cu_4I_4 clusters interconnected by 2-(*tert*-butylthio)-*N*-(pyridin-3-yl)acetamide, see: Cho, S.; Jeon, J.; Lee, S.; Kim, J.; Kim, T. H. *Chem.—Eur. J.* **2015**, *21*, 1439−1443.
(49) Su, C.-Y.; Kang, B.-S.; Sun, J. *Chem. Lett.* **1997**, 821−822.
(50) Song, R.-F.; Xie, Y.-B.; Li, J.-R.; Bu, X.-H. *CrystEngComm* **2005**, *7*, 249−254.
(51) Mochida, T.; Okazawa, K.; Horikoshi, R. *Dalton Trans.* **2006**, 693−704.
(52) Samanamú, C. R.; Lococo, P. M.; Woodul, W. D.; Richards, A. F. *Polyhedron* **2008**, *27*, 1463−1470.
(53) For other solid-state crystal-to-crystal transformations due to MeCN loss, see: (a) Kim, T. H.; Shin, Y. W.; Jung, J. H.; Kim, J. S.; Kim, J. *Angew. Chem., Int. Ed.* **2008**, *47*, 685−688. (b) Lee, J. Y.; Lee, S. Y.; Sim, W.; Park, K.-M.; Kim, J.; Lee, S. S. *J. Am. Chem. Soc.* **2008**, *130*, 6902−6903.
(54) Paulsson, H.; Berggrund, M.; Fischer, A.; Kloo, L. *Z. Anorg, Allg. Chem.* **2004**, *630*, 413−416.
(55) Knorr, M.; Guyon, F.; Kubicki, M. M.; Rousselin, Y.; Aly, S. M.; Harvey, P. D. *New J. Chem.* **2011**, *35*, 1184−1188.
(56) Xie, C.; Zhou, L.; Feng, W.; Wang, J.; Chen, W. *J. Mol. Struct.* **2009**, *921*, 132−136.
(57) (a) Hou, Q.; Yu, J.-H.; Xu, J.-N.; Yang, Q.-F.; Xu, J.-Q. *CrystEngComm* **2009**, *11*, 2452−2455. (b) Bi, M.; Li, G.; Hua, J.; Liu, Y.; Liu, X.; Hu, Y.; Shi, Z.; Feng, S. *Cryst. Growth Des.* **2007**, *7*, 2066−12070. (c) Zhang, Y.; Wu, T.; Liu, R.; Dou, T.; Bu, X.; Feng, P. *Cryst. Growth Des.* **2010**, *10*, 2047−2049. (d) Shan, X.-C.; Zhang, H.-B.;

DOI: 10.1021/acs.inorgchem.5b00327
Inorg. Chem. 2015, 54, 4076−4093

Chen, L.; Wu, M.-Y.; Jiang, F.-L.; Hong, M.-C. *Cryst. Growth Des.* **2013**, *13*, 1377−11381.
(58) For Cu_8I_8 clusters with other connectivities than those in **8**, see: (a) Cheng, Y.; Xu, P.; Ding, Y.-B.; Yin, Y.-G. *CrystEngComm* **2011**, *13*, 2644−2648. (b) Takemura, Y.; Nakajima, T.; Tanase, T. *Dalton Trans.* **2009**, 10231−10243. (c) Wang, J.; Zheng, S.-L.; Hu, S.; Zhang, Y.-H.; Tong, M.-L. *Inorg. Chem.* **2007**, *46*, 795−800.
(59) Tolman, C. A. *Chem. Rev.* **1977**, *77*, 313−348.
(60) Kim, T. H.; Lee, K. Y.; Shin, Y. W.; Moon, S.-T.; Park, K.-M.; Kim, J. S.; Kang, Y. *Inorg. Chem. Commun.* **2005**, *8*, 27−30.
(61) (a) Vitale, M.; Ryu, C. K.; Palke, W. E.; Ford, P. C. *Inorg. Chem.* **1994**, *33*, 561−566. (b) De Angelis, F.; Fantacci, S.; Sgamellotti, A.; Cariati, E.; Ugo, R.; Ford, P. C. *Inorg. Chem.* **2006**, *45*, 10576−10584. (c) For TDDFT calculations on Cu_4I_4(piperidine)$_4$, see: Jalilian, E.; Liao, R.-Z.; Himo, F.; Lidin, S. *Mater. Res. Bull.* **2011**, *46*, 1192−1196.
(62) (a) Vega, A.; Saillard, J. Y. *Inorg. Chem.* **2004**, *43*, 4012−4018. (b) Perruchas, S.; Tard, C. D.; Le Goff, X. F.; Fargues, A.; Garcia, A.; Kahlal, S.; Saillard, J.-Y.; Gacoin, T.; Boilot, J.-P. *Inorg. Chem.* **2011**, *50*, 10682−10692.
(63) (a) For a review on the photophysics of copper(I) compounds, see: Armaroli, N.; Accorsi, G.; Cardinali, F.; Listorti, A. *Top. Curr. Chem.* **2007**, *280*, 69−115. For general reviews on luminescent CPs, see: (b) Cui, Y.; Yue, Y.; Qian, G.; Chen, B. *Chem. Rev.* **2012**, *112*, 1126−1162. (c) Heine, J.; Müller-Buschbaum, K. *Chem. Soc. Rev.* **2013**, *42*, 9232−9242. (d) Allendorf, M. D.; Bauer, C. A.; Bhakta, R. K.; Houk, R. J. T. *Chem. Soc. Rev.* **2009**, *38*, 1330−1352.
(64) Knorr, M.; Guyon, F.; Khatyr, A.; Strohmann, C.; Allain, M.; Aly, S. M.; Lapprand, A.; Fortin, D.; Harvey, P. D. *Inorg. Chem.* **2012**, *51*, 9917−9934. (b) Knorr, M.; Khatyr, A.; Aleo, A.-D.; El Yaagoubi, A.; Strohmann, C.; Kubicki, M. M.; Rousselin, Y.; Aly, S.; Lapprand, A.; Fortin, D.; Harvey, P. D. *Cryst. Growth Des.* **2014**, *14*, 5373−5387.
(65) Piche, D.; Harvey, P. D. *Can. J. Chem.* **1994**, *72*, 705−713.
(66) Frisch, M. J. et al. *Gaussian 09*; Gaussian, Inc.: Wallingford, CT, 2004.
(67) (a) Hohenberg, P.; Kohn, W. *Phys. Rev.* **1964**, *136B*, 864−871. (b) Hohenberg, P.; Koh, W. *J. Phys. Rev.* **1965**, *140A*, 1133−1138.
(68) Parr, R. G.; Yang, W. *Density functional theory of atoms and molecules*; Oxford University Press: Oxford, U.K., 1989.
(69) Salahub, D. R.; Zerner, M. C. *The Challenge of d and f Electrons*; American Chemical Society: Washington, DC, 1989.
(70) Bauernschmitt, R.; Ahlrichs, R. *Chem. Phys. Lett.* **1996**, *256*, 454−464.
(71) Casida, M. E.; Jamorski, C.; Casida, K. C.; Salahub, D. R. *J. Chem. Phys.* **1998**, *108*, 4439−4449.
(72) Stratmann, R. E.; Scuseria, G. E.; Frisch, M. J. *J. Chem. Phys.* **1998**, *109*, 8218−8224.
(73) Lee, C.; Yang, W.; Parr, R. G. *Phys. Rev.* **1988**, *37 B*, 785−789.
(74) Miehlich, B.; Savin, A.; Stoll, H.; Preuss, H. *Chem. Phys. Lett.* **1989**, *157*, 200−206.
(75) (a) Binkley, J. S.; Pople, J. A.; Hehre, W. J. *J. Am. Chem. Soc.* **1980**, *102*, 939−947. (b) Gordon, M. S.; Binkley, J. S.; Pople, J. A.; Pietro, W. J.; Hehre, W. J. *J. Am. Chem. Soc.* **1982**, *104*, 2797−2803. (c) Pietro, W. J.; Francl, M. M.; Hehre, W. J.; Defrees, D. J.; Pople, J. A.; Binkley, J. S. *J. Am. Chem. Soc.* **1982**, *104*, 5039−5048.
(76) (a) Dobbs, K. D.; Hehre, W. J. *J. Comput. Chem.* **1986**, *7*, 359−378. (b) Dobbs, K. D.; Hehre, W. J. *J. Comput. Chem.* **1986**, *8*, 861−879. (c) Dobbs, K. D.; Hehre, W. J. *J. Comput. Chem.* **1986**, *8*, 880−893.
(77) O'Boyle, N. M.; Tenderholt, A. L.; Langner, K. M. *J. Comput. Chem.* **2008**, *29*, 839−845.
(78) Otwinowski, Z.; Minor, W. *Methods Enzymol.* **1997**, *276*, 307−326.
(79) *SAINT*; Bruker AXS Inc.: Madison, WI, 2008.
(80) Blessing, R. H. *Acta Crystallogr.* **1995**, *A51*, 33−38.
(81) Agilent Technologies. *CrysAlisPro*, release 01-02-2013; CrysAlis171.net.
(82) Sheldrick, G. M. *Acta Crystallogr.* **2008**, *A64*, 112−122.
(83) Altomare, A.; Cascarano, G.; Giacovazzo, C.; Guagliardi, A. *J. Appl. Crystallogr.* **1999**, *32*, 115−119.

DOI: 10.1021/acs.inorgchem.5b00327
Inorg. Chem. 2015, 54, 4076−4093